Ultralong-distance quantum correlations in three-terminal Josephson junctions

Régis Mélin
Université Grenoble Alpes, CNRS, Grenoble INP, Institut NEEL, 38000 Grenoble, France

(Received 14 March 2021; revised 22 June 2021; accepted 21 July 2021; published 2 August 2021)

The production of entangled pairs of electrons in ferromagnet-superconductor-ferromagnet or normal metal-superconductor-normal metal three-terminal structures has aroused considerable interest in the last twenty years. In these studies, the distance between the contacts is limited by the zero-energy superconducting coherence length. Here, we demonstrate nonlocality and quantum correlations in voltage-biased three-terminal Josephson junctions over the ultralong distance that exceeds the superconducting coherence length by orders of magnitude. The effect relies on the interplay between the time-periodic Floquet-Josephson dynamics, Cooper pair splitting, and long-range coupling similar to the two-terminal Tomasch effect. We find crossover between the "Floquet-Andreev quartets" (if the spatial separation is smaller than the superconducting coherence length) and the "ultralong-distance Floquet-Tomasch clusters of Cooper pairs" if the separation exceeds the superconducting coherence length, possibly reaching the same $\simeq 30$ μm as in the Tomasch experiments. The effect can be detected with DC-transport and zero-frequency quantum current-noise cross-correlation experiments, and it can be used for fundamental studies of superconducting quasiparticle quantum coherence in the circuits of quantum engineering.

DOI: 10.1103/PhysRevB.104.075402

I. INTRODUCTION

The recent developments in the field of quantum engineering allow manipulation of long-range quantum objects with a few degrees of freedom. Superconductivity is a platform for fundamental studies of large-scale quantum systems [1–4] and for assembling quantum processors [5]. Superconducting quasiparticles can generally propagate over the entire sample and quasiparticle poisoning [6–13] turns out to severely limit the range of quantum mechanical coherence in superconductors. Superconducting devices with three or more terminals could naturally be used for fundamental studies of coherent quasiparticle propagation. Propagation over R_0 across one of the superconducting leads, say S_c, trivially requires two interfaces, one with S_a and the other one with S_b, thus forming S_a-S_c-S_b double Josephson junction where S_a and S_b are laterally connected to S_c at distance R_0. The field of multiterminal Josephson junctions [14–39] has recently been enriched with the discovery of nontrivial topology [40–48] and topology in the time-periodic Floquet dynamics [49–51].

In view of these recent contributions, we address here the fundamental question of the range of nonlocality and quantum correlations in the three-terminal devices formed with the two Josephson junction oscillators S_a-S_c and S_c-S_b sharing the grounded S_c. In spite of the well-known classical synchronization of macroscopic Josephson junction circuits [52,53], the present paper surprisingly demonstrates mesoscopic quantum correlations in three-terminal Josephson junctions at the "ultralong-distance" that exceeds the superconducting coherence length $\xi_{\rm ball}(0)$ by orders of magnitude.

Specifically, we consider a S_a-dot-S_c-dot-S_b three-terminal Josephson junction made with the BCS superconductors S_a, S_b, and S_c and two quantum dots [see Figs. 1(a)–1(c)]. This physical system has the following features: (i) the time-periodic Floquet-Josephson dynamics with single characteristic frequency if biasing is at commensurate voltages [14–22]; (ii) the nonlocal electron-hole or hole-electron conversions, i.e., Cooper pair splitting [54–77]; and (iii) the long-range quasiparticle propagation above the gap between the two remote quantum dots separated by the distance R_0. Then, we demonstrate that (i), (ii), and (iii) automatically imply large-scale quantum-mechanical clusters of Cooper pairs between the constituting S-dot-S junctions, even if the distance R_0 between them is much larger than the zero-energy superconducting coherence length $\xi_{\rm ball}(0)$, i.e., if $R_0 \gg \xi_{\rm ball}(0)$. These clusters can be viewed as being "the elementary quantum particles" that are exchanged between the two Floquet-Josephson junctions in a three-terminal configuration. Figure 1(d) features real-space representation of the lowest-order four-Cooper pair cluster corresponding to the "ultralong-distance Floquet-Tomasch octets."

In the absence of bias voltage, all superconducting leads are grounded and the three-terminal S_a-S_c-S_b Josephson junction [14,23–27] can be phase-biased with appropriate superconducting loops. The Andreev bound states [78–88] are then coupled by the overlapping evanescent Bogoliubov-de Gennes wave functions at a double interface, forming "Andreev molecules" with avoided crossings in their spectra, see Refs. [23,24]. At equilibrium, nonlocality is limited by the superconducting coherence length $\xi_{\rm ball}(0)$ as a function of the distance R_0 between the S_a-S_c and S_c-S_b interfaces [23–27].

We note that a DC-Josephson-like resonance appears if the three superconducting terminals (S_a, S_c, S_b) are biased on the

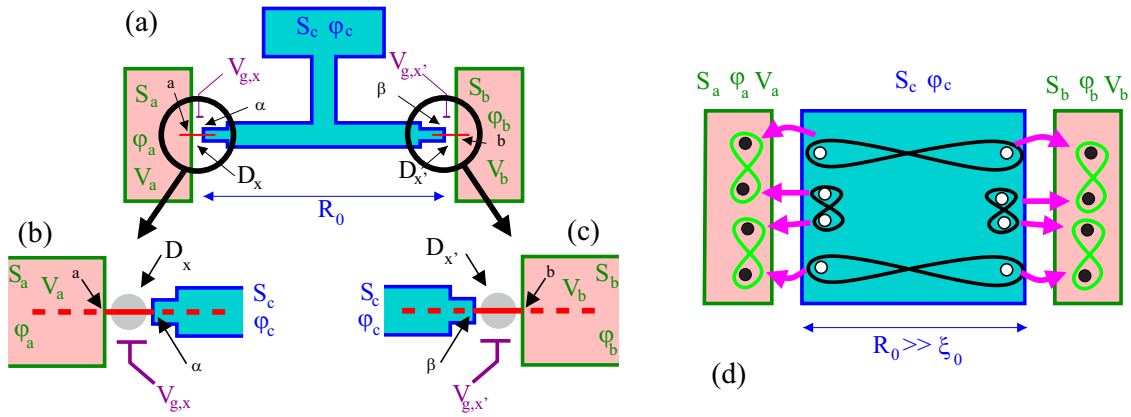

FIG. 1. The device considered in the paper, consisting of the three-terminal S_a-D_x-S_c-$D_{x'}$-S_b Josephson junction biased on the quartet line at the voltages $(V_a, V_c, V_b) = (V, 0, -V)$. The two quantum dots D_x and $D_{x'}$ make distance R_0 between them. (a) features the entire device, and (b) and (c) show enlargements around the regions of the D_x and $D_{x'}$ quantum dots formed with semiconducting nanowires [31], with the gate voltages $V_{g,x}$ and $V_{g,x'}$. (d) shows schematically the Cooper pair cluster of the ultralong-distance Floquet-Tomasch octets, see also Fig. 4. The separation R_0 between the contacts can be much larger than the zero-energy coherence length $\xi_0 \equiv \xi_{\rm ball}(0)$.

"quartet line" [14]:

$$(V_a, V_c, V_b) = (V, 0, -V). \tag{1}$$

The resulting Josephson relations $\varphi_a(t) = \varphi_a + 2eVt/\hbar$, $\varphi_b(t) = \varphi_b - 2eVt/\hbar$ and $\varphi_c(t) = \varphi_c$ for the superconducting phase variables at time t imply the static "quartet phase variable" $\varphi_q = \varphi_a(t) + \varphi_b(t) - 2\varphi_c(t) = \varphi_a + \varphi_b - 2\varphi_c$ [14]. This yields the quartet current-phase relation $I_{c,q} \sin \varphi_q$ in the limit of low values of the contact transparencies. The three recent experiments of the Grenoble [30], Weizmann Institute [31], and Harvard [32] groups show all signs of compatibility with the theory of the quartets [14–21], in addition to other experiments [33–39] on multiterminal Josephson junctions. The reason why some experiments report the quartets while others do not is maybe a complex matter of the materials and geometry.

The present paper focuses on the range of the quartets at finite bias voltage V being a fraction of the superconducting gap Δ. Concerning propagation across S_c between the two Josephson junctions, the Tomasch effect was experimentally shown in Refs. [89–91] to produce oscillations in the density of states of the superconducting quasiparticles in a two-terminal configuration, as a result of the finite superconducting film thickness reaching 33.2 μm in the experimental Ref. [91]. The "Tomasch effect" [89–91] and the model proposed by McMillan and Anderson [92] provide sensitivity on the thin film boundary conditions, corresponding to the two-terminal nonlocal density-phase response, see also the contribution of Wolfram and Lehman [93]. The here considered three-terminal "Floquet-Tomasch effect for the Cooper pair clusters" couples one junction to the phase drop at the other junction according to the nonlocal current-phase response and it does not involve the same microscopic quantum process as the three-terminal density of state oscillations. The former is DC-current current response and the latter corresponds to AC-density oscillations. Nonlocality and quantum correlations are obtained in the Floquet-Tomasch effect over the ultralong-distance $R_0 \gg \xi_{\rm ball}(0)$ that is orders of magnitude larger than at equilibrium.

This ultralong-distance effect contrasts with the F_aSF_b ferromagnet-superconductor-ferromagnet and the N_aSN_b normal metal-superconductor-normal metal beam splitters, where nonlocality and quantum correlations are limited by the superconducting coherence length $\xi_{\rm ball}(0)$, see, for instance, Refs. [54–77].

The paper is organized as follows. The physical picture is presented in Sec. II. The model and methods are presented in Sec. III. Analytical model calculations are presented in Sec. IV. Section V deals with presentation of the numerical results. Perspectives on noise measurements are discussed in Sec. VI. Summary of the paper is provided in Sec. VII.

II. PHYSICAL PICTURE

We first present the basics of Cooper pair splitting and nonlocality limited by the superconducting coherence length, see Refs. [54–77]. The range of Cooper pair splitting is introduced in Sec. II A for three-terminal F_aSF_b and N_aSN_b devices. Next, we proceed further in Sec. II B with the ultralong-distance Floquet-Tomasch effect in a three-terminal S_a-D_x-S_c-$D_{x'}$-S_b Josephson junction, where D_x and $D_{x'}$ denote the two quantum dots.

A. Nonlocality of Cooper pair splitting

This section introduces nonlocality and quantum correlations in a three-terminal F_aSF_b or N_aSN_b device, in connection with Cooper pair splitting, see Refs. [54–77].

Andreev reflection [78] at a normal metal-superconductor (NS) interface converts the supercurrent carried by Cooper pairs in S into normal current in N. Namely, spin-up electron from N is Andreev-reflected as a spin-down hole and a Cooper pair is transmitted into the condensate. The semiclassical trajectories of the incoming electron and outgoing hole are separated on the NS interface by less than the superconducting coherence length $\xi_{\rm ball}(0)$, which is why Andreev reflection is nonlocal at the scale of the superconducting coherence length.

The experimental evidence [54–61] for the theoretical prediction of nonlocal Andreev reflection [62–77] involves three-terminal configurations, such as the above mentioned F_aSF_b or N_aSN_b devices.

Regarding the range of Cooper pair splitting in three-terminal F_aSF_b and N_aSN_b devices, the zero-energy superconducting coherence length $\xi_{\rm ball}(0)$ is given by

$$\xi_{\rm ball}(0) = \frac{\hbar v_F}{\Delta} \tag{2}$$

in the ballistic limit, where v_F is the Fermi velocity. This "size of a Cooper pair" is energy/frequency-ω-sensitive:

$$\xi_{\rm ball}(\omega - i\eta_S) = \frac{\hbar v_F}{\sqrt{\Delta^2 - (\omega - i\eta_S)^2}}, \tag{3}$$

where v_F is the Fermi velocity. Equation (3) diverges as the energy ω goes to the superconducting gap Δ, see also Ref. [94] for the nonlocal conductance $\mathscr{G}_{a,b} = \partial I_a/\partial V_b$ at arbitrary bias voltage V_b with respect to the superconducting gap.

B. Ultralong-distance Floquet-Tomasch effect

The introduction of "the Feynman diagrams" in calculations of the light-matter interaction was not only useful to represent the quantum processes, but it also yielded considerable shortcuts in the calculation of those scattering amplitudes. Here, the diagrams yield intuitive explanations and simple physical pictures for the numerical results presented in Sec. V. Those diagrams represent the time evolution of the electrons, holes and the conversions between them, scattering back and forth between the different interfaces.

This section considers nonlocality in the S_a-D_x-S_c-$D_{x'}$-S_b three-terminal Josephson junction on Figs. 1(a)–1(c), which is biased according to Eq. (1) in a voltage-V range that is significant fraction of the superconducting gap Δ, typically $eV \sim \Delta/2$. Specifically, we detail the microscopic processes, starting with the nonlocal pair amplitude, and next proceeding further with the Floquet-Andreev and the Floquet-Tomasch contributions to the current, finally uncovering the ultralong-distance Floquet-Tomasch octets. We demonstrate in Appendix A that the Floquet-Tomasch effect for the current of pairs in a three-terminal Josephson junction and the two-terminal density of state oscillations in the Tomasch effect [89–93] share the ultralong-distance nonlocality, but the corresponding quantum processes are inequivalent. Thus, the mechanism for the two-terminal density of state oscillations in the Tomasch effect [89–93] cannot be advocated to be at the origin of the ultralong-distance current of pairs in the three-terminal Josephson junction. In the first place, in the three-terminal configuration, the quantum processes coupling the density of states at one contact to the pairs at the other contacts are AC at the lowest-order in the tunneling amplitudes, and thus, they cannot be put forward as an explanation to the calculated three-terminal DC-current of quartets and higher order clusters of Cooper pairs.

Figures 2(a) and 2(b) show the energy diagram for the lowest-order pair amplitude between the quantum dots D_x and $D_{x'}$, corresponding to conversion of "spin-up electron on the dot D_x" into "spin-down hole on the dot $D_{x'}$."

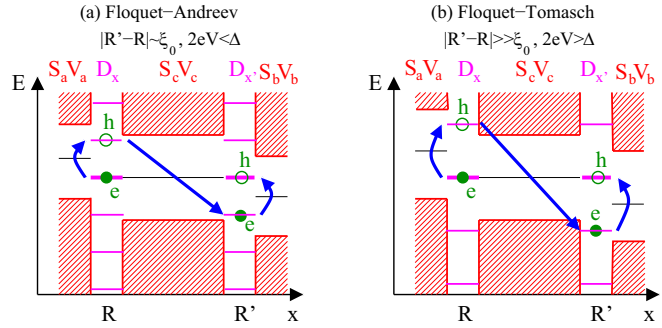

FIG. 2. Schematic Floquet-Andreev pair amplitude for $2eV < \Delta$ (a) and Floquet-Tomasch pair amplitude for $2eV > \Delta$ (b). Both panels show conversion of a spin-up electron (e) on dot D_x as a hole in the spin-down band (h) on dot $D_{x'}$. Floquet-Andreev on panel a involves subgap propagation over $R_0 = |\mathbf{R}' - \mathbf{R}| \lesssim \xi_{\rm ball}(0)$ and Floquet-Tomasch on (b) implies propagation above the gap if $R_0 \gg \xi_{\rm ball}(0)$.

The processes in Figs. 2(a) and 2(b) start with electron-hole conversion at the S_a-D_x-S_c Josephson junction: local Floquet-Andreev reflection first increases the energy by 2 eV (i.e., the energy of a Cooper pair taken from the lead S_a biased at the voltage V). The process continues with nonlocal propagation from D_x to $D_{x'}$ across S_c in the hole-electron channel. Next, "local" inverse-Floquet hole-electron conversion takes place at the S_c-$D_{x'}$-S_b Josephson junction. In the final state, spin-down hole is produced at zero energy on the quantum dot $D_{x'}$.

The condition $|2eV| < \Delta$ on the bias voltage V [see Fig. 2(a)] implies conversion in the hole-electron channel over the superconducting coherence length $\xi_{\rm ball}(\omega)$, see Eq. (3). This subgap process is referred to as "the Floquet-Andreev quartet pair amplitude."

Conversely, $|2eV| > \Delta$ in Fig. 2(b) implies nonlocal hole-electron conversion above the gap of S_c. This process is limited by the mesoscopic phase coherence length l_φ of the superconducting quasiparticles, and it is referred to as "the ultralong-distance Floquet-Tomasch pair amplitude" [see the forthcoming Eqs. (11)–(18)], in analogy with the Tomasch effect [89–92] mentioned above in the Introduction.

Emergence of the ultralong-distance Floquet-Tomasch pair amplitude if $|2eV| > \Delta$ implies ultralong-distance nonlocality over $R_0 \sim l_\varphi$, and quantum correlations in the φ_q-sensitive current, which is considered now.

Now, we "close the loop" in Figs. 3(a) and 3(b) with final zero-energy hole-electron conversion from $D_{x'}$ to D_x. The resulting φ_q-sensitive Floquet-Andreev quartet current is limited by the superconducting coherence length $\xi_{\rm ball}(0)$, independently on whether $|2eV| < \Delta$ or $|2eV| > \Delta$.

Finally, we consider the higher order process of the ultralong-distance Floquet-Tomasch octets having $\sin(2\varphi_q)$ sensitivity and range limited by l_φ. Figure 4 shows the corresponding diagram, see also Fig. 1(d). Two nonlocal and two local hole-electron conversions are involved: (i) nonlocally from D_x to $D_{x'}$ and from $D_{x'}$ to D_x across S_c, and (ii) locally between each S_a and S_b, the D_x and $D_{x'}$ quantum dots and S_c. Overall, the resulting $\sin(2\varphi_q)$-sensitive octet current appears if the distance R_0 between the remote S_a-D_x-S_b and S_c-$D_{x'}$-S_b junctions reaches $R_0 \sim l_\varphi$, such that $l_\varphi \gg \xi_{\rm ball}(0)$.

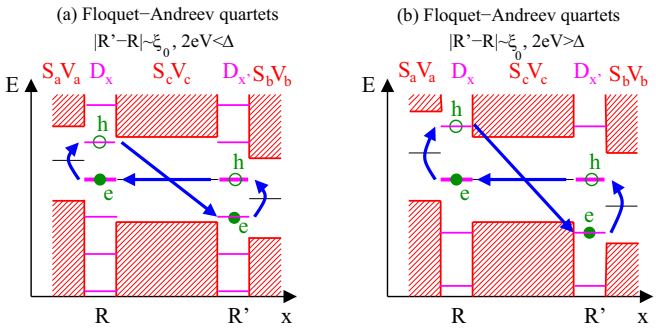

FIG. 3. Schematic Floquet-Andreev DC-transport diagrams for $2eV < \Delta$ (a) and $2eV > \Delta$ (b). Both processes correspond to "closing" the pair amplitude diagrams on Fig. 2 by addition of propagation at zero energy from $D_{x'}$ to D_x, thus forming a process contributing to the DC current. Both panels have distance $R_0 = |\mathbf{R}' - \mathbf{R}| \lesssim \xi_{\rm ball}(0)$ between D_x and $D_{x'}$, and φ_q-quartet phase sensitivity.

We conclude that Fig. 4 provides microscopic picture for the proposed ultralong-distance Floquet-Tomasch octets as an eight-fermion cluster originating from four Cooper pairs, see also Fig. 1(d).

This physical picture suggests crossover as R_0 increases from below to above $\xi_{\rm ball}(0)$, i.e., from "the dominant $\sin\varphi_q$ of the Floquet-Andreev quartets over $\xi_{\rm ball}(0)$" to "the dominant $\sin(2\varphi_q)$ of the ultralong-distance Floquet-Tomasch octets over l_φ." A crossover to the higher order-n clusters of Cooper pairs is expected as the voltage values is reduced below $\Delta/2n$ (with n an integer).

We proceed further with the models and methods in Sec. III, next with the analytical results in Sec. IV and finally the theory is put to the test of the numerical calculations in Sec. V.

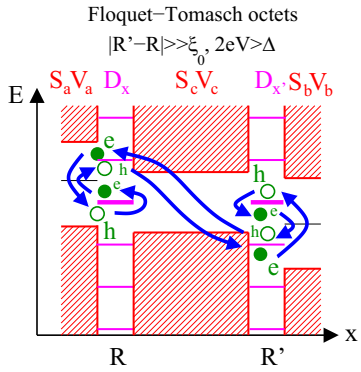

FIG. 4. Schematic higher order ultralong-distance Floquet-Tomasch octet DC-current diagram for $2eV > \Delta$. This process takes two pairs from S_a at $V_a = +V$, two pairs from S_b at $V_b = -V$, split two of them and locally transfers the two others into the grounded S_c, thus with $2\varphi_q$-quartet phase sensitivity. The distance between D_x and $D_{x'}$ is $R_0 = |\mathbf{R}' - \mathbf{R}| \gg \xi_{\rm ball}(0)$. Comparing to Fig. 3, we deduce crossover from the φ_q quartets to the $2\varphi_q$ octets as R_0 is increased from $R_0 \lesssim \xi_{\rm ball}(0)$ [see Fig. 3(b)] to $R_0 \gg \xi_{\rm ball}(0)$ (in the present figure). This process is also shown schematically in Fig. 1(d).

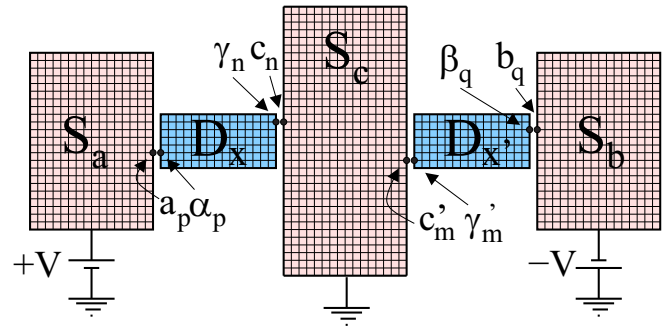

FIG. 5. Schematic tight-binding model of the considered S_a-D_x-S_c-$D_{x'}$-S_b three-terminal Josephson junction containing two quantum dots D_x and $D_{x'}$. The quantum dots have finite dimension on this figure. This is "the model I."

III. MODEL AND METHODS

We start in Sec. III A with a brief description of the models used in the paper, i.e., the geometry and the Hamiltonians. Next, we present in Sec. III B a central ingredient of the model, i.e., the connection between the Dynes parameter and the mesoscopic phase coherence length of the superconducting quasiparticles. The methods are mentioned in Sec. III C.

A. Geometry and Hamiltonians

Now, we present the geometry and the Hamiltonians. Figures 1(a)–1(c) show the device geometry: the T-shaped grounded superconducting lead S_c connected *via* the two quantum dots D_x and $D_{x'}$ to S_a and S_b biased at $V_{a,b} = \pm V$. Those figures represent quasi-one-dimensional semiconducting nanowire quantum dots similar to Ref. [31]. The distance between D_x and $D_{x'}$ is denoted by $R_0 = |\mathbf{R}' - \mathbf{R}|$.

Now, we provide the Hamiltonians. The BCS Hamiltonian of each infinite superconducting lead with gap Δ and phase φ is given by

$$\mathscr{H}_{\rm BCS} = -W \sum_{\langle i,j\rangle} \sum_{\sigma} (c^+_{i,\sigma} c_{j,\sigma} + c^+_{j,\sigma} c_{i,\sigma}) \tag{4}$$

$$- \Delta \sum_i (e^{i\varphi} c^+_{i,\uparrow} c^+_{i,\downarrow} + e^{-i\varphi} c_{i,\downarrow} c_{i,\uparrow}), \tag{5}$$

where, again, $\sigma = \uparrow, \downarrow$ is the projection of the spin along the quantization axis, and φ takes the values φ_a, φ_b, or φ_c according to which of the superconducting lead S_a, S_b, or S_c is considered. The notation $\langle i, j\rangle$ in Eq. (4) stands for pairs of neighboring sites on a three-dimensional (3D) tight-binding lattice, and the label i in Eq. (5) runs over all tight-binding sites.

The tunnel Hamiltonian couples the tight-binding sites on both sides of the contacts:

$$\mathscr{H}_T = -J \sum_{\langle i,j\rangle} \sum_{\sigma} (c^+_{i,\sigma} c_{j,\sigma} + c^+_{j,\sigma} c_{j,\sigma}), \tag{6}$$

where $\langle i, j\rangle$ in Eq. (6) denotes the pairs of corresponding tight-binding sites on both sides of the two-dimensional (2D) interface.

The Hamiltonian of a direct-gap semiconductor making the quantum dots in Fig. 5 is inspired by Ref. [95]. We take the

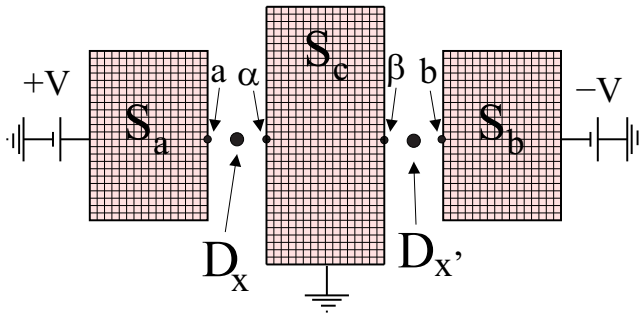

FIG. 6. Schematic tight-binding model of the considered S_a-D_x-S_c-$D_{x'}$-S_b three-terminal Josephson junction containing two quantum dots D_x and $D_{x'}$. The quantum dots are zero-dimensional (0D) on this figure. This is "the reduced model II."

following Hamiltonian in the infinite 3D bulk limit:

$$\mathscr{H}_1 = \sum_{\mathbf{q}} \sum_{\sigma} \frac{|\mathbf{q}|^2}{2m_e} a^+_{\mathbf{q},\sigma} a_{\mathbf{q},\sigma} - \sum_{\mathbf{q}} \sum_{\sigma} \left(E_g + \frac{|\mathbf{q}|^2}{2m_h} \right) b^+_{\mathbf{q},\sigma} b_{\mathbf{q},\sigma}, \tag{7}$$

where $a^+_{\mathbf{q},\sigma}$ or $b^+_{\mathbf{q},\sigma}$ create spin-σ fermions with the wave vector $\mathbf{q}$ in the conduction or valence band, and E_g is the value of the direct gap. We will use in Sec. IV the fact that the dispersion relations appearing in Eq. (7) have extrema at the wave vector $q^* = 0$.

Considering the $\langle a, \alpha \rangle$ pair of tight-binding sites making the contact at the interface between the superconductor S_a and the quantum dot D_x (see Fig. 5), the local creation operator $c^+_{\alpha,\sigma}$ on the surface D_x is defined as a sum over the quantum numbers n_1 and n_2 of the $a^+_{n_1,\sigma}$ and $b^+_{n_2,\sigma}$ creation operators associated to both conduction and valence bands, respectively:

$$c^+_{\alpha,\sigma} = \sum_{n_1} \varphi^*_{a,n_1}(\mathbf{R}_\alpha) a^+_{n_1,\sigma} + \sum_{n_2} \varphi^*_{b,n_2}(\mathbf{R}_\alpha) b^+_{n_2,\sigma}, \tag{8}$$

where we assumed a quantum dot with finite dimension, and the tight-binding site labeled by α is at the space coordinate $\mathbf{R}_\alpha$. In Eq. (8), the quantum numbers n_1 and n_2 label the states of the quantum dot with finite dimension, possibly with irregularities in its shape, and having Eq. (7) as its bulk Hamiltonian. The notations $\varphi_{a,n_1}(\mathbf{R}_\alpha)$ and $\varphi_{b,n_2}(\mathbf{R}_\alpha)$ stand for the corresponding conduction and valence band wave functions.

The zero-dimensional (0D) quantum dot in Fig. 6 has level at zero energy. Thus the corresponding Hamiltonian is $\mathscr{H}'_1 = 0$.

The quantum dots are connected with highly transparent interfaces to the leads, which is why the Coulomb interaction is included neither in Eq. (7) nor in $\mathscr{H}'_1 = 0$. For instance, the recent experiments [39] on Andreev molecules [23–27] do not seem to require Coulomb interactions as a central ingredient, because of the highly transparent interfaces.

Zero temperature is assumed throughout the paper. Nontrivial quasiparticle populations can be produced at zero temperature by driving normal current between two attached normal leads. An interesting theoretical and experimental question is to address whether driving normal current can result in change of sign of the quartet critical current, similarly to two terminals, see Refs. [96,97].

The scattering approach or the Keldysh Green's functions [98] were complementary used in the past to address superconducting junctions, see for instance Refs. [99–101] for a single superconducting weak link. Both approaches have their own advantages. For instance, the scattering matrix calculations and the wave-function approach allow for semiclassical calculations, see Refs. [48,102]. Microscopic Green's functions produce efficient algorithms to address the general conditions of high transparencies and large current bias, see for instance Ref. [94]. In the following, we rely on the Keldysh Green's functions, on the basis of the algorithms that were developed over the last few years [17–19,21,48].

We also implement the simplifying assumption of a ballistic superconductor, similarly to the McMillan-Anderson and the Wolfram-Lehman papers [92,93] on the Tomasch effect [89–91]. Taking the ballistic limit yields considerable simplifications in the calculations, see below. Disorder in the superconductors could be introduced in the future on the basis of the Usadel equations [103]. Another possible approach is to assume perturbation theory in the strength of the nonlocal processes between the two quantum dots, see the forthcoming Sec. IV, and to average over disorder the pairs of nonlocal Green's functions connecting both quantum dots. The 16 Nambu components of the advanced-advanced transmission modes (see Ref. [20]) would then have to be generalized to the Keldysh contour and to energy outside the superconducting gap.

B. The mesoscopic phase coherence length of the superconducting quasiparticles

In this section, we relate the mesoscopic phase coherence length l_φ of the superconducting quasiparticles to the Dynes parameter η_S [17,104–107].

By the time-energy uncertainty relation, and by the correspondence between the time and length scales, a characteristic length $\hbar v_F/E_0$ is associated to any energy scale E_0. To the Fermi energy ϵ_F is associated the Fermi wave-length λ_F, which is much smaller than the superconducting coherence length $\xi_{\rm ball}(0)$ that is related to the superconducting gap Δ. The characteristic length l_φ is conjugate to the Dynes parameter η_S, and it phenomenologically accounts for the quantum-to-classical crossover of the propagating superconducting quasiparticles, due to inelastic scattering and energy relaxation. Then, l_φ is much larger than the superconducting coherence length $\xi_{\rm ball}(0)$, i.e., $l_\varphi \gg \xi_{\rm ball}(0)$, because the Dynes parameter η_S is much smaller than the superconducting gap Δ, i.e., $\eta_S \ll \Delta$, see Refs. [17,104–107]. The length scale l_φ has to crossover to its normal-state value $\hbar v_F/\eta_S$ as the energy ω crosses-over above $\omega \gtrsim 2\Delta$. This l_φ naturally receives the interpretation of defining the "limit of the quantum world" as far as the superconducting quasiparticle propagation is concerned.

Now, within this phenomenological "Dynes picture," we provide analytical expressions for the mesoscopic phase coherence length l_φ of the superconducting quasiparticles as a function of the energy ω.

The evanescent Bogoliubov-de Gennes wave functions decay exponentially like $\sim \exp(-R/\xi_{\rm ball}(\omega - i\eta_S))$ from the interface at the subgap energy $|\omega| < \Delta$, see also the Green's

function given by Eq. (B3). Then, the superconducting coherence length $\xi_{\rm ball}(\omega - i\eta_S)$ can be continued to energies $|\omega| > \Delta$ outside the gap, and it has the following real and imaginary parts:

$$\frac{1}{\xi_{\rm ball}(\omega - i\eta_S)} = {\rm Re}\left(\frac{1}{\xi_{\rm ball}(\omega - i\eta_S)}\right) + i\,{\rm Im}\left(\frac{1}{\xi_{\rm ball}(\omega - i\eta_S)}\right), \tag{9}$$

which yields damping and oscillations:

$$\exp\left(-\frac{R}{\xi_{\rm ball}(\omega - i\eta_S)}\right) = \exp\left[-R\,{\rm Re}\left(\frac{1}{\xi_{\rm ball}(\omega - i\eta_S)}\right)\right] \times \exp\left[-i\,R\,{\rm Im}\left(\frac{1}{\xi_{\rm ball}(\omega - i\eta_S)}\right)\right]. \tag{10}$$

We define the inverse damping length as

$$\frac{1}{l_\varphi} = {\rm Re}\left[\frac{1}{\xi_{\rm ball}(\omega - i\eta_S)}\right], \tag{11}$$

with $|\omega| > \Delta$.

We note that ${\rm Re}\sqrt{\Delta^2 - (\omega - i\eta_S)^2} = \rho\cos(\theta/2)$, where $\rho^2\exp(i\theta) = \Delta^2 - \omega^2 + \eta_S^2 + 2i\eta_S\omega$. Using $\cos\theta = 2\cos^2(\theta/2) - 1$ leads to

$${\rm Re}\sqrt{\Delta^2 - (\omega - i\eta_S)^2} = \frac{1}{\sqrt{2}}\left\{\left[\left(\Delta^2 - \omega^2 + \eta_S^2\right)^2 + 4\eta_S^2\omega^2\right]^{1/2} + \Delta^2 - \omega^2 + \eta_S^2\right\}^{1/2}. \tag{12}$$

Assuming $\eta_S \ll \Delta$ and $|\omega| > \Delta$ yields

$$\left\{\left(\Delta^2 - \omega^2 + \eta_S^2\right)^2 + 4\eta_S^2\omega^2\right\}^{1/2} \simeq |\Delta^2 - \omega^2| + \eta_S^2\frac{\Delta^2 + \omega^2}{|\Delta^2 - \omega^2|} \tag{13}$$

and

$$\left\{\left[\left(\Delta^2 - \omega^2 + \eta_S^2\right)^2 + 4\eta_S^2\omega^2\right]^{1/2} + \Delta^2 - \omega^2 + \eta_S^2\right\}^{1/2} \simeq \left\{\eta_S^2\frac{\Delta^2 + \omega^2 + |\Delta^2 - \omega^2|}{|\Delta^2 - \omega^2|}\right\}^{1/2}, \tag{14}$$

where we used $\Delta^2 - \omega^2 + |\Delta^2 - \omega^2| = 0$ if $|\omega| > \Delta$. The following is deduced:

$${\rm Re}\sqrt{\Delta^2 - (\omega - i\eta_S)^2} \simeq \eta_S\frac{|\omega|}{[\omega^2 - \Delta^2]^{1/2}}, \tag{15}$$

and $1/l_\varphi$ is given by

$$\frac{1}{l_\varphi} \simeq \frac{\eta_S}{\hbar v_F} \times \frac{|\omega|}{[\omega^2 - \Delta^2]^{1/2}}. \tag{16}$$

Then, $l_\varphi \approx l_\varphi^{\rm max}$ if the energy ω takes the typical value $|\omega| \approx 2\Delta$:

$$l_\varphi^{(\rm max)} = \frac{\hbar v_F}{\eta_S}. \tag{17}$$

This yields

$$\frac{l_\varphi^{(\rm max)}}{\xi_{\rm ball}(0)} = \frac{\Delta}{\eta_S}, \tag{18}$$

where $l_\varphi^{(\rm max)}$ is expressed in units of the zero-energy superconducting coherence length $\xi_{\rm ball}(0)$, see Eq. (2). The Dynes ratio $\eta_S/\Delta \ll 1$ is small in the experiments [104–107], which implies the ultralong-distance effect corresponding to $l_\varphi^{(\rm max)}/\xi_{\rm ball}(0) \gg 1$ in Eq. (18).

Thus Eq. (18) supports the idea presented in the Introduction, i.e., within this Dynes picture, the mesoscopic phase coherence length l_φ of the superconducting quasiparticles is orders of magnitude larger than the zero-energy superconducting coherence length $\xi_{\rm ball}(0)$ in a typical energy window that can roughly be estimated as $|\omega| \approx 2\Delta$. This typical spectral window for emergence of the ultralong-distance Floquet-Tomasch effect reflects the coexistence of both features of the normal and superconducting states, i.e., long l_φ and sizable nonlocal Andreev processes.

Controlling the electromagnetic environment as in Ref. [106] can reduce the value of the Dynes parameter η_S by orders of magnitude, and produce large value of l_φ according to Eqs. (11)–(18). This can also be used to rule out the coupling to the electromagnetic environment as the origin of the quartet line. In the previous Grenoble [30] and Weizmann group experiments [31], a device fabricated with remote junctions did not produce the quartet line in spite of the same electromagnetic environment as in the device with close junctions.

C. Methods

The analytical and numerical calculations presented in Secs. IV and V respectively are based on the Keldysh Green's functions. Details about the methods are provided in Appendix B.

IV. ANALYTICAL RESULTS

In this section, we assume that the quantum dots are fabricated with direct-gap semiconductors [see Eq. (7)], and we map "the model I" in Fig. 5 onto "the reduced model II" in Fig. 6. We also provide analytical results demonstrating the Floquet-Andreev quartets and the ultralong-distance Floquet-Tomasch octets, discuss the absence of dephasing in propagation between the two interface and explain why the ultralong-distance effect appears both for the two-terminal density of states in the Tomasch experiments [89–91], and for the pair current in the here considered three-terminal Josephson junction. However, the quantum processes are distinct from each other and it turns out that the nonlocal coupling between the density of states at one contact and the pairs at the other contact is AC in the three-terminal Josephson junction.

Specifically, starting with the model I in Fig. 5, we assume that the Nambu Green's function of each quantum dot D_x or $D_{x'}$ fulfills the following "generalized star-triangle relation," i.e., we propose the following for the quantum dot D_x:

$$\hat{g}_{\alpha_{p_1},\alpha_{p_2}} = \tilde{g}_{\alpha_{p_1},x}\tilde{g}_{x,x}\tilde{g}_{x,\alpha_{p_2}}, \tag{19}$$

$$\hat{g}_{\alpha_{p_1},\gamma_{n_2}} = \tilde{g}_{\alpha_{p_1},x}\tilde{g}_{x,x}\tilde{g}_{x,\gamma_{n_2}}. \tag{20}$$

The assumption of resonance at zero energy implies $\tilde{g}^A_{x,x} \sim 1/(\omega - i\eta)$, see the discussion following Eq. (B1) in Appendix B. We consider that the quantum dots have minimum

at the wave-vector $q^* = 0$ in their dispersion relation, see Eq. (7). We assume that the contact dimension is small compared to $2\pi/q^*$ and that the size of the quantum dots is small compared to the decay length of the evanescent wave functions on the dot. Then, $\hat{g}_{\alpha_{p_1},\alpha_{p_2}}$ and $\hat{g}_{\alpha_{p_1},\gamma_{n_2}}$ are roughly independent on p_1, p_2, and $\tilde{g}$ is the matrix square root of the residue in Eq. (B2).

The Green's functions are matrices in Nambu and in the enlarged space of the harmonics of the Josephson frequency. The labels p_1, p_2 running over the tight-binding sites at the interfaces are now made implicit [see Eqs. (19) and (20)].

The fully dressed Green's function $\tilde{G}_{x,x}$ on the dot D_x can be "expanded in nonlocality" according to

$$\tilde{G}_{x,x} = \tilde{L}_{x,x} \tag{21}$$

$$+\tilde{L}_{x,x}\tilde{K}_{x,x'}\tilde{L}_{x',x'}\tilde{K}_{x',x}\tilde{L}_{x,x} \tag{22}$$

$$+\tilde{L}_{x,x}\tilde{K}_{x,x'}\tilde{L}_{x',x'}\tilde{K}_{x',x}\tilde{L}_{x,x}\tilde{K}_{x,x'}\tilde{L}_{x',x'}\tilde{K}_{x',x}\tilde{L}_{x,x} \tag{23}$$

$$+\ldots, \tag{24}$$

where $\tilde{L}_{x,x}$ and $\tilde{L}_{x',x'}$ describe "local" dressing at the S_a-D_x-S_c and S_c-$D_{x'}$-S_b junctions, and the matrices $\tilde{K}_{x,x'}$ and $\tilde{K}_{x',x}$ correspond to nonlocal propagation from x to x' and from x' to x respectively, see Appendix C. An expansion similar to Eqs. (21)–(24) was previously developed for the nonlocal conductance of F_aSF_b or N_aSN_b beam splitters, see Ref. [74]. Here, the small parameter for nonlocality of the Floquet-Andreev quartets is $\epsilon_0 = \exp[-2R_0/\xi_{\rm ball}(0)]$, due to transmission of quasiparticles *via* evanescent states in the subgap energy window. The small parameter for the Floquet-Tomasch octets is $\epsilon_\varphi = \exp[-2R_0/l_\varphi(\omega)]$ instead of the previous ϵ_0, corresponding to propagation *via* plane waves in a spectral window above the gap of S_c, and damping over the mesoscopic phase coherence length $l_\varphi(\omega)$, see Eqs. (11)–(16).

The first term in Eq. (21) does not couple the two quantum dots. The Keldysh component of the second term in Eq. (22) is the following:

$$\Sigma_{a,\alpha}G^{+,-}_{\alpha,a} \simeq (\Sigma_{a,\alpha}\tilde{g}_{\alpha,x}\tilde{L}_{x,x}\tilde{K}_{x,x'}\tilde{L}_{x',x'}\tilde{K}_{x',x}\tilde{L}_{x,x}\tilde{g}_{x,\alpha}\Sigma_{\alpha,a}g_{a,a})^{+,-}. \tag{25}$$

Specifying the Nambu labels corresponding to anomalous propagation between D_x and $D_{x'}$ leads to

$$(\Sigma_{a,\alpha}G^{+,-}_{\alpha,a})_{(1,1)} \simeq (\Sigma_{a,\alpha,(1,1)}\tilde{g}_{\alpha,x,(1,1)}\tilde{L}_{x,x,(1,1)}\tilde{K}_{x,x',(1,2)}\tilde{L}_{x',x',(2,1)}\tilde{K}_{x',x,(1,2)}\tilde{L}_{x,x,(2,2)}\tilde{g}_{x,\alpha,(2,2)}\Sigma_{\alpha,a,(2,2)}g_{a,a,(2,1)})^{+,-}. \tag{26}$$

Within this approximation, the Floquet-Tomasch quartets and octets propagate a pair of nonlocal Green's functions between the two quantum dots, where Eq. (26) also captures "local" dressing by multiple Andreev reflections at each S-dot-S Josephson junction.

The Floquet-Andreev quartets correspond to

$$(\Sigma_{a,\alpha}G^{+,-}_{\alpha,a})_{(1,1)/(0,0)} \simeq (\Sigma_{a,\alpha,(1,1)/(0,1)}\tilde{g}_{\alpha,x,(1,1)/(1,1)}\tilde{L}_{x,x,(1,1)/(1,1)}\tilde{K}_{x,x',(1,2)/(1,1)}\tilde{L}_{x',x',(2,1)/(1,-1)}$$
$$\times\,\tilde{K}_{x',x,(1,2)/(-1,-1)}\tilde{L}_{x,x,(2,2)/(-1,-1)}\tilde{g}_{x,\alpha,(2,2)/(-1,-1)}\Sigma_{\alpha,a,(2,2)/(-1,0)}g_{a,a,(2,1)/(0,0)})^{+,-}, \tag{27}$$

where the "$(\tau_1,\tau_2)/(n_1,n_2)$" labels are used for the Nambu and Floquet labels respectively. Both $\tilde{K}_{x,x'}$ and $\tilde{K}_{x',x}$ entering Eq. (27) are of order ϵ_0 if $R_0 \gtrsim \xi_{\rm ball}(0)$, due to the corresponding dominant contribution of the subgap energy window. Thus $(\Sigma_{a,\alpha}G^{+,-}_{\alpha,a})_{(1,1)}$ in Eq. (26) is of order $(\epsilon_0)^2$.

The Floquet-Tomasch Keldysh Green's function is given by

$$(\Sigma_{a,\alpha}G^{+,-}_{\alpha,a})_{(1,1)/(0,0)} \simeq (\Sigma_{a,\alpha,(1,1)/(0,1)}\tilde{g}_{\alpha,x,(1,1)/(1,1)}\tilde{L}_{x,x,(1,1)/(1,3)}\tilde{K}_{x,x',(1,2)/(3,3)}\tilde{L}_{x',x',(2,1)/(3,1)}\tilde{K}_{x',x,(1,2)/(1,1)}$$
$$\times\,\tilde{L}_{x,x,(2,2)/(1,-1)}\tilde{g}_{x,\alpha,(2,2)/(-1,-1)}\Sigma_{\alpha,a,(2,2)/(-1,0)}g_{a,a,(2,1)/(0,0)})^{+,-}, \tag{28}$$

where $\tilde{K}_{x,x',(1,2)}$ and $\tilde{K}_{x',x,(1,2)}$ entering Eq. (28) are both of order ε_φ if $R_0 \gtrsim l_\varphi$. Thus, $(\Sigma_{a,\alpha}G^{+,-}_{\alpha,a})_{(1,1)}$ in Eq. (28) is of order $(\varepsilon_\varphi)^2$.

Equations (27) and (28) imply that the current I_q on the quartet line is expressed as summation over c_1, c_2 and c_1', c_2' at the D_x-S_c and S_c-$D_{x'}$ interfaces respectively, see Fig. 5: $I_q = \sum_{c_1,c_2,c_1',c_2'} I_{c_1,c_2,c_1',c_2'}$. Then, Eq. (B4) in Appendix B yields

$$I_q = \sum_{c_1,c_2,c_1',c_2'} I'_{c_1,c_2,c_1',c_2'} \cos\left[k_F R_{c_1,c_1'}\right]\cos\left[k_F R_{c_2,c_2'}\right]. \tag{29}$$

Gathering the Green's functions in a pairwise manner [108,109] yields $I_q \simeq \sum_{c,c'} I_{c,c,c',c'}$ and

$$I_q \simeq \frac{k_F}{2\pi}\int_{R_0}^{R_0+2\pi/k_F} I_q(R)dR, \tag{30}$$

where $I_q(R)$ is the spectral current of the "reduced model II in Fig. 6" at the distance R between the 0D quantum dots.

Thus the use of direct-gap semiconductor quantum dots allows replacing "the multichannel contacts of the model I" by "the 0D quantum dots of the reduced model II" while averaging over ψ_F in Eq. (B4). We also singled-out the Floquet-Andreev quartet and the ultralong-distance Floquet-Tomasch octet contributions to the current, which supports the physical picture of the preceding Secs. II and III, and the numerical results of the forthcoming Sec. V.

We also note that biasing at $eV = \pm\Delta/2$ produces coinciding gap edge singularities of S_a and S_b. This is expected to result in large values for the quartet and octet critical currents $I_{q,c}\sin\varphi_q$ and $I_{o,c}\sin(2\varphi_q)$, as for perfectly transparent contacts. The following scaling form of $|I_{q,c}|$ and $|I_{o,c}|$ at the

voltages $eV = \pm\Delta/2$ can be conjectured:

$$|I_{q,c}| \approx \frac{e}{\hbar}\exp\left(-\frac{2R_0}{\xi_{\rm ball}(0)}\right), \tag{31}$$

$$|I_{o,c}| \approx \frac{e}{\hbar}\exp\left(-\frac{2R_0}{l_\varphi}\right). \tag{32}$$

Both $|I_{q,c}|$ and $|I_{o,c}|$ are expected to be reduced if the bias voltage is detuned from $\pm\Delta/e$. This Eq. (32) will further be considered in the next section on the numerical data.

Finally, we underline consistency with Ref. [92] regarding robustness with respect to dephasing between the corresponding pairs of Green's function. The superconducting Green's function $\hat{g}^A_{\mathbf{x},\mathbf{y}}$ in Eq. (B4) is rewritten as

$$\hat{g}^A_{\mathbf{x},\mathbf{y}} = \frac{1}{W}\frac{1}{k_F R}\exp\left\{\left(-\frac{R}{\xi_{\rm ball}(\omega - i\eta_S)}\right)\right\} \tag{33}$$

$$\times\left[\cos\psi_F \hat{\mathscr{M}}_{\cos}\left(\frac{\omega}{\Delta}\right) + \sin\psi_F \hat{\mathscr{M}}_{\sin}\left(\frac{\omega}{\Delta}\right)\right], \tag{34}$$

where

$$\hat{\mathscr{M}}_{\cos}\left(\frac{\omega}{\Delta}\right) = \frac{1}{\sqrt{\Delta^2 - (\omega - i\eta_S)^2}}\begin{pmatrix} -(\omega - i\eta_S) & \Delta e^{i\varphi} \\ \Delta e^{-i\varphi} & -(\omega - i\eta_S)\end{pmatrix}, \tag{35}$$

$$\hat{\mathscr{M}}_{\sin}\left(\frac{\omega}{\Delta}\right) = \begin{pmatrix} -1 & 0 \\ 0 & 1\end{pmatrix}, \tag{36}$$

and $R = |\mathbf{x} - \mathbf{y}|$ is the distance between $\mathbf{x}$ and $\mathbf{y}$. We assume that the Fermi wavelength $\lambda_F = 2\pi/k_F$ is much smaller than all other length scales:

$$\mathrm{Re}\left[\frac{1}{\xi_{\rm ball}(\omega - i\eta_S)}\right] \ll k_F, \tag{37}$$

$$\mathrm{Im}\left[\frac{1}{\xi_{\rm ball}(\omega - i\eta_S)}\right] \ll k_F. \tag{38}$$

In addition, the characteristic dimension R_1 of the quantum dot is such that $R_1 \ll \xi_{\rm ball}(0)$, which implies that the oscillations are not washed-out by extended contacts. Then, using the notation

$$\langle\langle \ldots \rangle\rangle = \frac{k_F}{2\pi}\int_{R_0}^{R_0 + 2\pi/k_F} dR \tag{39}$$

for averaging over R in the interval $[R_0, R_0 + 2\pi/k_F]$, see Eq. (30), we express the averaging of the pairs of Nambu Green's functions as follows:

$$\left\langle\left\langle \hat{g}^A_{\mathbf{x},\mathbf{y}}\left(\frac{\omega_1}{\Delta}\right) \otimes \hat{g}^A_{\mathbf{y},\mathbf{x}}\left(\frac{\omega_2}{\Delta}\right)\right\rangle\right\rangle \simeq \frac{1}{2W^2}\frac{1}{(k_F R)^2}\exp\left\{\left(-\frac{R}{\xi_{\rm ball}(\omega_1 - i\eta_S)}\right)\right\}\exp\left\{\left(-\frac{R}{\xi_{\rm ball}(\omega_2 - i\eta_S)}\right)\right\}$$

$$\times\left[\hat{\mathscr{M}}_{\cos}\left(\frac{\omega_1}{\Delta}\right) \otimes \hat{\mathscr{M}}_{\cos}\left(\frac{\omega_2}{\Delta}\right) + \hat{\mathscr{M}}_{\sin}\left(\frac{\omega_1}{\Delta}\right) \otimes \hat{\mathscr{M}}_{\sin}\left(\frac{\omega_2}{\Delta}\right)\right]. \tag{40}$$

The corresponding anomalous components involve one or two nonlocal Andreev electron-hole or hole-electron conversion. They take sizeable values if ω_1, ω_2 are typically in the energy window $0 < |\omega_1|, |\omega_2| \lesssim 2\Delta$ instead of being strictly inside the gap according to $0 < |\omega_1|, |\omega_2| < \Delta$. This implies that the ultralong-distance effect holds for all of the quantum electron-hole conversion processes captured by Eq. (40), and being characterized by different sets of the corresponding 16 Nambu labels. As a consequence, both the density of state oscillations of the two-terminal Tomasch effect and the clusters of Cooper pairs in the three-terminal Josephson junction are characterized by the corresponding ultralong-distance coupling, see also Appendix A where the demonstration starts from the different point of view of the open boundary conditions considered by Wolfram and Lehman in Ref. [93]. However, it is also shown in this Appendix A that the coupling between the density of states at one contact and the pairs at the other contact is AC in the three-terminal Josephson junction. Thus, those AC density of state oscillations in a three-terminal Josephson junction cannot explain the following numerical data on the DC-current of clusters of Cooper pairs also with three superconducting terminals.

To interpret the finite electron-hole or hole-electron conversion amplitude above the gap, in a characteristic spectral window $|\omega| \lesssim 2\Delta$, we refer to Fig. 7(a) in the Blonder-Tinkham-Klapwijk approach [110], showing the sizable Andreev reflection conductance of a highly-transparent normal metal-superconductor junction as a function of voltage V such that $|eV| \lesssim 2\Delta$.

In addition, the quasiparticles and pairs in the Tomasch oscillations in the two-terminal density of states [89–91] co-propagate over ultralong-distance, and they can be referred to as "the correlations among three fermions" [111], i.e. between a single quasiparticle and a pair. Conversely, two copropagating pairs correspond to "the so-called quartets" in three-terminal Josephson junctions [14]. A possibility is to speculate that enhanced condensation energy could be produced by those propagating Nambu modes acting like a "glue," in addition to the mean field BCS pairing. Indeed, it would be interesting to consider analogies with the theory of the collective modes [112–114], and to examine whether those "triplets" or "quartets" can possibly give rise to a collective state upon taking the Coulomb interaction or strong disorder into account.

V. NUMERICAL RESULTS

In this section, we provide selection of numerical data for the reduced model II, defined in the above Sec. IV.

We successively introduce the calculations and present the ultralong-distance effect, see Figs. 7 and 8. Next, we present the crossover from the Floquet-Andreev quartets to the ultralong-distance Floquet-Tomasch octets in the quartet phase sensitivity of the current, as the distance between the dots is increased from $R_0/\xi_{\rm ball}(0) \lesssim 1$ to $R_0/\xi_{\rm ball}(0) \gtrsim 1$ and to $R_0/\xi_{\rm ball}(0) \gg 1$, see Figs. 9 and 10.

The current of the S_a-D_x-S_c-$D_{x'}$-S_b double quantum dot three-terminal Josephson junction is obtained from the fully

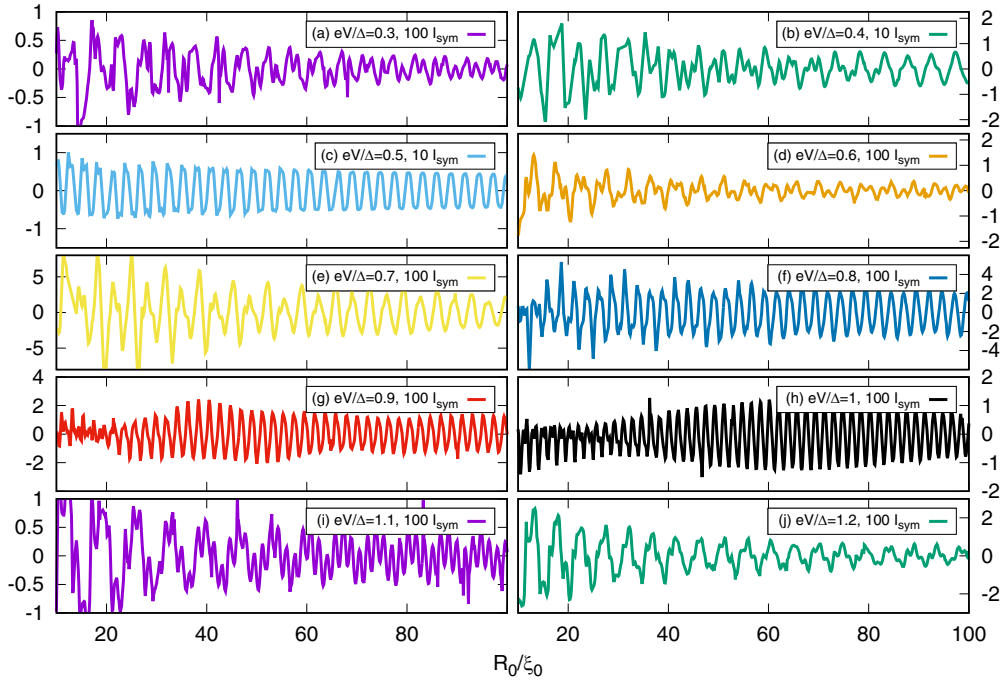

FIG. 7. The ultralong-distance effect. The figure shows the symmetric current $I_{\rm sym}$ defined by Eq. (41) for a S_a-D_x-S_c-$D_{x'}$-S_b three-terminal Josephson junction biased at the voltages $(V_a, V_b, V_c) = (V, -V, 0)$. [(a)–(j)] correspond to $eV/\Delta = 0.3,\ 0.4,\ 0.5,\ 0.6,\ 0.7,\ 0.8,\ 0.9,\ 1,\ 1.1,$ and 1.2. The couplings between the quantum dots and the superconducting leads are the following: $\Gamma_{x,a}/\Delta = \Gamma_{x',b}/\Delta = 0.25$ and $\Gamma_{x,\alpha}/\Delta = \Gamma_{x',\beta}/\Delta = 1$. The quartet phase is $\varphi_q/2\pi = 0.1$. The Dynes parameter is $\eta_S/\Delta = 10^{-3}$, thus with $l_\varphi^{(\max)} = 10^3\xi_0$, where ξ_0 is a short notation for $\xi_{\rm ball}(0)$. The quartet phase variable is set to $\varphi_q/2\pi = 0.1$, see the forthcoming Fig. 9 for the φ_q sensitivity of the quartet current at fixed separation $R_0/\xi_{\rm ball}(0)$. The current is in units of $e\Delta/\hbar$.

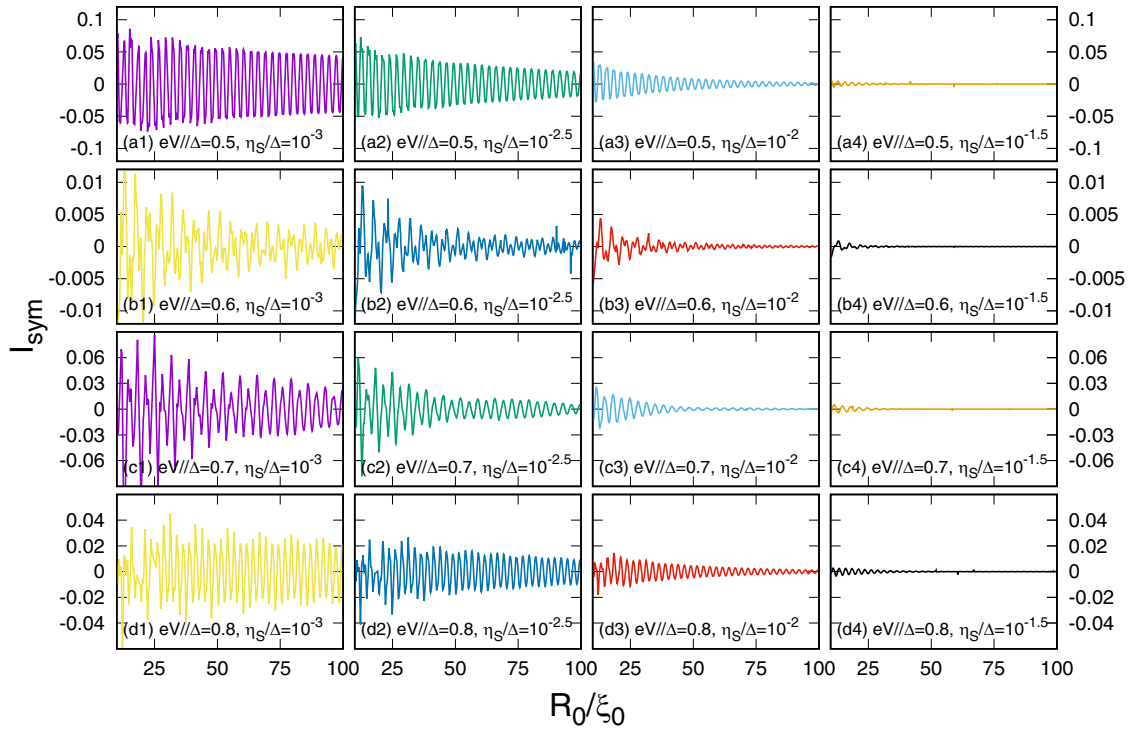

FIG. 8. The effect of the Dynes parameter on the ultralong-distance effect. The figure shows the symmetric current $I_{\rm sym}$ defined by Eq. (41) for a S_a-D_x-S_c-$D_{x'}$-S_b three-terminal Josephson junction biased at the voltages $(V_a, V_b, V_c) = (V, -V, 0)$. Panels a1-a4, b1-b4, c1-c4 and d1-d4 correspond to $eV/\Delta = 0.5,\ 0.6,\ 0.7,\ 0.8.$ respectively. The values of the Dynes parameters are the following: $\eta_S/\Delta = 10^{-3}$ (a1, b1, c1, d1), $\eta_S/\Delta = 10^{-2.5}$ (a2, b2, c2, d2), $\eta_S/\Delta = 10^{-2}$ (a3, b3, c3, d3), and $\eta_S/\Delta = 10^{-1.5}$ (a4, b4, c4, d4). The other parameters are identical to Fig. 7. The current is in units of $e\Delta/\hbar$.

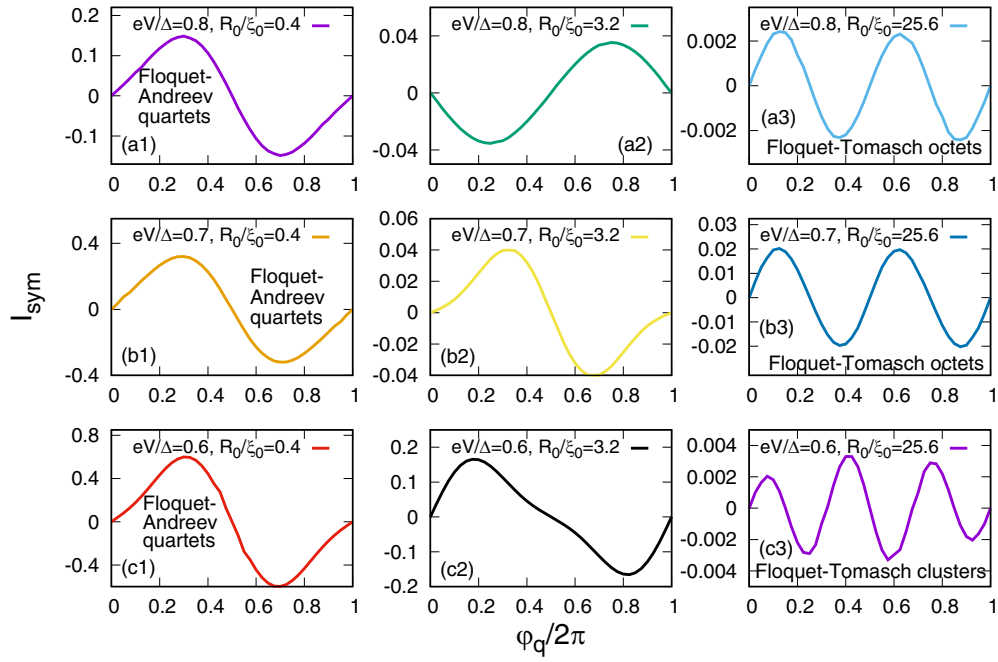

FIG. 9. The crossover from the Floquet-Andreev quartets to the ultralong-distance Floquet-Tomasch octets. The figure shows the symmetric current $I_{\rm sym}$ defined by Eq. (41) for a S_a-D_x-S_c-$D_{x'}$-S_b three-terminal Josephson junction biased at the voltages $(V_a,\ V_b,\ V_c) = (V,\ -V,\ 0)$, as a function of $\varphi_q/2\pi$ on the x axis. The voltage values are $eV/\Delta = 0.5,\ 0.4,\ 0.3$ and $R_0/\xi_{\rm ball}(0) = 0.4,\ 3.2,\ 25.6$. The couplings between the quantum dots and the superconducting leads are the following: $\Gamma_{x,a}/\Delta = \Gamma_{x',b}/\Delta = 0.25$ and $\Gamma_{x,\alpha}/\Delta = \Gamma_{x',\beta}/\Delta = 1$. The Dynes parameter is $\eta_S/\Delta = 10^{-3}$, thus with $l_\varphi^{(\max)} = 10^3\xi_0$, where ξ_0 is a short notation for $\xi_{\rm ball}(0)$. The current is in units of $e\Delta/\hbar$.

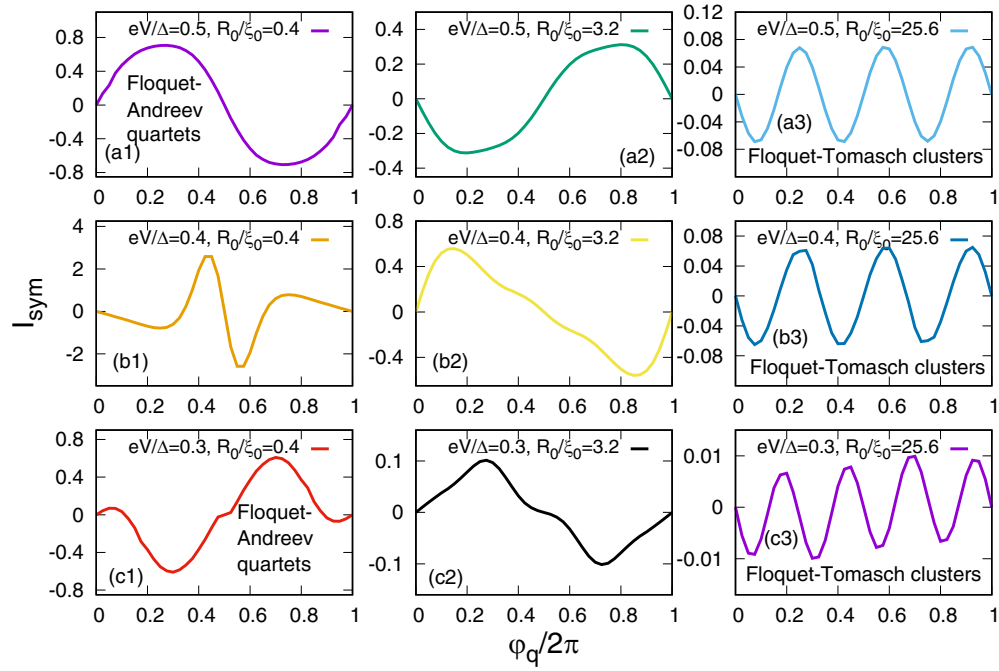

FIG. 10. The crossover from the Floquet-Andreev quartets to the ultralong-distance Floquet-Tomasch clusters. The figure shows the symmetric current $I_{\rm sym}$ defined by Eq. (41) for a S_a-D_x-S_c-$D_{x'}$-S_b three-terminal Josephson junction biased at the voltages $(V_a,\ V_b,\ V_c) = (V,\ -V,\ 0)$, as a function of $\varphi_q/2\pi$ on the x-axis. The voltage values are $eV/\Delta = 0.5,\ 0.4,\ 0.3$ and $R_0/\xi_{\rm ball}(0) = 0.4,\ 3.2,\ 25.6$. The couplings between the quantum dots and the superconducting leads are the following: $\Gamma_{x,a}/\Delta = \Gamma_{x',b}/\Delta = 0.25$ and $\Gamma_{x,\alpha}/\Delta = \Gamma_{x',\beta}/\Delta = 1$. The Dynes parameter is $\eta_S/\Delta = 10^{-3}$, thus with $l_\varphi^{(\max)} = 10^3\xi_0$, where ξ_0 is a short notation for $\xi_{\rm ball}(0)$.

dressed Dyson-Keldysh equations to all orders in the tunneling amplitudes. Concerning the algorithms, the code is based on numerically exact implementation of the Dyson and Dyson-Keldysh Eqs. (B6) and (B7), see Appendix B. The Dyson Eq. (B6) is solved with recursive Green's functions in energy [100] and sparse matrix algorithms are used for the matrix products. Details about the algorithms can be found in the Appendix of Ref. [18].

Based on symmetry arguments [15,16], we implement the hopping amplitudes $J_{a,x} = J_{b,x'}$ and $J_{\alpha,x} = J_{\beta,x'}$, thus with $\Gamma_{x,a} = \Gamma_{x',b}$ and $\Gamma_{x,\alpha} = \Gamma_{x',\beta}$ for the normal-state linewidth broadening parameters $\Gamma_n = J_n^2/W$. Then, we evaluate the current of the clusters of Cooper pairs as

$$I_{\rm sym}\left(\frac{R_0}{\xi_{\rm ball}(0)},\ \frac{eV}{\Delta},\ \frac{\varphi_q}{2\pi}\right) = I_a\left(\frac{R_0}{\xi_{\rm ball}(0)},\ \frac{eV}{\Delta},\ \frac{\varphi_q}{2\pi}\right) + I_b\left(\frac{R_0}{\xi_{\rm ball}(0)},\ \frac{eV}{\Delta},\ \frac{\varphi_q}{2\pi}\right), \quad (41)$$

where the currents I_a and I_b are transmitted into S_a and S_b, and $I_{\rm sym}$ in Eq. (41) is averaged over $k_F R$ according to Eq. (30).

We start with the sensitivity of $I_{\rm sym}(R_0/\xi_{\rm ball}(0), eV/\Delta,\ \varphi_q/2\pi)$ on the distance $R_0/\xi_{\rm ball}(0)$ between the quantum dots D_x and $D_{x'}$. The data on Fig. 7 show the current $I_{\rm sym}$ as a function of $R_0/\xi_{\rm ball}(0)$ at the fixed quartet phase $\varphi_q/2\pi = 0.1$ and for the reduced voltage values from $eV/\Delta = 0.3$ to $eV/\Delta = 1.2$ on panels (a)–(j), respectively. The numerical data in Fig. 7 feature complex pattern of the Floquet-Tomasch oscillations. The beatings are interpreted as interference between the wave vectors of the quantum dot level Floquet replica. The numerical data in Fig. 7 fully confirm the physical picture of Sec. II regarding the ultralong-distance Floquet-Tomasch oscillations. The value $\eta_S/\Delta = 10^{-3}$ of the Dynes parameter used in Fig. 7 implies $l_\varphi^{\rm max}/\xi_{\rm ball}(0) = 10^3$, see Eqs. (11)–(16). This is compatible with emergence of sizable $I_{\rm sym}(R_0/\xi_{\rm ball}(0), eV/\Delta,\ \varphi_q/2\pi)$ at $R_0/\xi_{\rm ball}(0) = 100$ in Fig. 7. By contrast, R_0 is limited by $R_0 \lesssim \xi_{\rm ball}(0)$ in the recently considered Andreev molecules with all superconducting leads grounded [14,23–27], and in the F_aSF_b and N_aSN_b Cooper pair beam splitters, see Refs. [54–77]. We also note that, strictly speaking, $\xi_{\rm ball}(0)$ given by Eq. (2) and $l_\varphi^{\rm max}$ given by Eq. (17) are two independent length scales, in the sense that $l_\varphi^{\rm max}$ is not proportional to $\xi_{\rm ball}(0)$. The current $I_{\rm sym}$ was averaged over the oscillations at the scale of the Fermi wave-length $\lambda_F = 2\pi/k_F$ according to Eq. (30). Then, $\xi_{\rm ball}(0)$ is the smallest length scale to which the calculated $I_{\rm sym}$ couples and it is illustrative to plot $I_{\rm sym}$ as a function of $R_0/\xi_{\rm ball}(0)$.

Figure 8 illustrates the effect of the Dynes parameter on the current $I_{\rm sym}$. In this figure, the Dynes parameter η_S/Δ ranges from $\eta_S/\Delta = 10^{-3}$ [in panels (a1), (b1), (c1), and (d1)] to $\eta_S/\Delta = 10^{-2.5}$ [in panels (a2), (b2), (c2), and (d2)], $\eta_S/\Delta = 10^{-2}$ [in panels (a3), (b3), (c3), and d(3)], and $\eta_S/\Delta = 10^{-1.5}$ [in panels (a4), (b4), (c4), and (d4)]. The voltage values are $eV/\Delta = 0.5,\ 0.6,\ 0.7,\ 0.8$ on panels (a1)–(a4), (b1)–(b4), (c1)–(c4), and (d1)–(d4), respectively. It is concluded that the range of the Floquet-Tomasch effect is strongly reduced by increasing the Dynes parameter from $\eta_S/\Delta = 10^{-3}$ to $10^{-1.5}$, in agreement with the physical arguments presented in the preceding Secs. II, III, and IV.

We also deduce from the y scales in Fig. 7 that the current $I_{\rm sym}$ reaches maximum around $eV/\Delta \approx 1/2$, i.e., $I_{\rm sym}$ for $eV/\Delta = 0.4,\ 0.5$ in Figs. 7(b) and 7(c) is one order of magnitude larger than for $eV/\Delta = 0.3,\ 0.6$ in Figs. 7(a) and 7(d). The strong enhancement of $I_{\rm sym}$ at $eV/\Delta = 1/2$ is interpreted as the coinciding upper and lower gap edge singularities of S_a and S_b which are biased at $\pm V = \pm\Delta/2e$, as if the contact transparencies would be enhanced by orders of magnitude in this voltage window, see the remarks related to Eqs. (31) and (32) in the previous Sec. IV.

It is also visible in Figs. 8 and 9 that the current $I_{\rm sym}$ is larger for $eV/\Delta = 0.7$ than for $eV/\Delta = 0.8$. The voltage dependence of $I_{\rm sym}$ is indeed expected to be nonmonotonic, because of the interplay between the voltage-V sensitive peaks in the density of states coming from the quantum dot Floquet replica, and the BCS gap edge singularities, see the diagrams in Fig. 4.

The crossover from the Andreev quartets to the ultralong-distance Floquet-Tomasch octets was proposed in Sec. II as $R_0/\xi_{\rm ball}(0)$ is increased from $R_0/\xi_{\rm ball}(0) \lesssim 1$ to $R_0/\xi_{\rm ball}(0) \gtrsim 1$ and next to $R_0/\xi_{\rm ball}(0) \gg 1$. Figures 9 and 10 show how $I_{\rm sym}(R_0/\xi_{\rm ball}(0), eV/\Delta,\ \varphi_q/2\pi)$ depends on the quartet phase $\varphi_q/2\pi$ at fixed values of the reduced voltage eV/Δ and distance $R_0/\xi_{\rm ball}(0)$ between the quantum dots. The values $eV/\Delta = 0.5,\ 0.4,\ 0.3$ and $R_0/\xi_{\rm ball}(0) = 0.4,\ 3.2,\ 25.6$ are used in Fig. 9, $eV/\Delta = 0.5,\ 0.4,\ 0.3$ and $R_0/\xi_{\rm ball}(0) = 0.4,\ 3.2,\ 25.6$ are used in Fig. 10.

In general, the symmetric current $I_{\rm sym}$ has dominant quartet, octet or higher order φ_q sensitivity, namely $I_{\rm sym} \sim \sin\varphi_q$, $I_{\rm sym} \sim \sin(2\varphi_q)$, or $I_{\rm sym} \sim \sin(n\varphi_q)$, respectively.

The voltage $eV/\Delta = 0.8$ in Figs. 9(a1), 9(a2), and 9(a3) confirms the crossover from the $\sin\varphi_q$ Andreev quartets to the $\sin(2\varphi_q)$ ultralong-distance Floquet-Tomasch octets as $R_0/\xi_{\rm ball}(0)$ is increased from $R_0/\xi_{\rm ball}(0) = 0.8$ to $R_0/\xi_{\rm ball}(0) = 3.2$ and to $R_0/\xi_{\rm ball}(0) = 25.6$. The dominant $\sin\varphi_q$ and $-\sin\varphi_q$ are obtained for the small $R_0/\xi_{\rm ball}(0) = 0.4$ and for the intermediate $R_0/\xi_{\rm ball}(0) = 3.2$ in Figs. 9(a1) and 9(a2), while the dominant $\sin(2\varphi_q)$ of the ultralong-distance Floquet-Tomasch octets is obtained for $R_0/\xi_{\rm ball}(0) = 25.6$ in Fig. 9(a3).

We also proposed in Sec. II emergence of higher order harmonics in the current-quartet phase relation as eV/Δ is reduced. To illustrate this point, we now reduce the bias voltage to $eV/\Delta = 0.7$ [see Figs. 9(b1), 9(b2), and 9(b3)] and to $eV/\Delta = 0.6$ [see Figs. 9(c1), 9(c2), and 9(c3)]. The following voltage values are also used on Fig. 10: $eV/\Delta = 0.5$ [see Figs. 10(a1), 10(a2), and 10(a3)], $eV/\Delta = 0.4$ (see Figs. 10(b1), 10(b2), and 10(b3)] and $eV/\Delta = 0.3$ [see Figs. 10(c1), 10(c2), and 10(c3)]. The dominant $\sin(3\varphi_q)$ harmonics emerges for $eV/\Delta = 0.6,\ R_0/\xi_{\rm ball}(0) = 25.8$ in Fig. 9(c3) and for $eV/\Delta = 0.5,\ R_0/\xi_{\rm ball}(0) = 25.8, eV/\Delta = 0.4,\ R_0/\xi_{\rm ball}(0) = 25.8$ in Figs. 10(a3) and 10(b3). The higher order $\sin(4\varphi_q)$ harmonics is also obtained for $eV/\Delta = 0.3,\ R_0/\xi_{\rm ball}(0) = 25.8$ in Fig. 10(c3).

We note consistency with our previous results for a single 0D quantum dot [18]. Namely, $R_0/\xi_{\rm ball}(0) = 0.4$ and $R_0/\xi_{\rm ball}(0) = 3.2$ in Figs. 9(a1), 9(a2), and 9(c1) and in Figs. 10(a1), 10(a2), and 10(c1) feature the 0-to-π and π-to-0 crossovers which were found in our previous Ref. [18]

To summarize, the numerical calculations confirm the physical picture of Sec. II, Appendix A and the analytical results of Sec. IV regarding the following items: (i) the ultralong range of the effect and the way it depends on the Dynes parameter ratio η_S/Δ, (ii) the sensitivity on the quartet phase φ_q, i.e., the crossover from the Andreev quartets to the ultralong-distance Floquet-Tomasch octets as $R_0/\xi_{\rm ball}(0)$ is increased from $R_0/\xi_{\rm ball}(0) \lesssim 1$ to $R_0/\xi_{\rm ball}(0) \gtrsim 1$ and to $R_0/\xi_{\rm ball}(0) \gg 1$, (iii) the voltage dependence of the effect, i.e., the emergence of higher order harmonics at smaller values of the voltage eV/Δ, and (iv) the emergence of large ultralong-distance signal if $eV \simeq \pm\Delta/2$, which becomes weaker if eV is tuned away from $\pm\Delta/2$.

VI. DISCUSSION

In this section, we discuss consequences for probing the "quantumness" of the Floquet-Tomasch clusters of Cooper pairs with quantum current-noise cross-correlations. We distinguish between theory (see Sec. VI A) and possible experiments (see Sec. VI B).

A. Quantum current-noise cross-correlations

The price to pay for nonlocal clusters of Cooper pairs over the ultralong-distance $R_0 \sim l_\varphi$ is apparently to renounce to a "good Floquet qubit." Considering that the bias voltage energy eV is much smaller than the superconducting gap Δ, the Floquet resonance linewidth broadening δ is limited by multiple Andreev reflections [17,19,21,48], at least in the absence of "extrinsic" mechanism of relaxation [17]. We previously reported [17,19,21,48] that $\delta \sim \exp(-c\Delta/eV)$ with c of order unity, i.e., the linewidth broadening is exponentially small as eV/Δ is reduced. But here, the coupling to the continua of quasiparticles above the gap produces significant broadening of the Floquet resonances and small coherence time [17,19,21,48] at higher voltage values, from $eV/\Delta = 0.3$ to $eV/\Delta = 1.2$ in Figs. 7–9.

This "poor Floquet qu-bit" does however not preclude emergence of quantum correlations at the ultralong distance $R_0 \sim l_\varphi$, because the Cooper pair clusters are composite objects made of both the "locally transmitted" and "nonlocally split" Cooper pairs, see Fig. 1(d). It is known that, in general, breaking Cooper pairs produces quantum mechanical correlations and entanglement, see the F_aSF_b and the N_aSN_b beam splitters [64–77]. Nonvanishingly small zero-frequency quantum current-noise cross-correlations $S_{a,b} \neq 0$ in a S_a-dot-S_c-dot-S_b three-terminal Josephson junction at the ultralong $R_0 \sim l_\varphi$ is a possibility for experimental demonstration of the quantum nature of the ultralong-distance Cooper pair clusters.

In fact, the quantum current-noise cross-correlation kernel

$$S_{a,b}(\tau) = \hbar \int d\tau' K_{a,b}(\tau,\tau') \tag{42}$$

was calculated by many authors, see for instance Ref. [101] and Eqs. (15)–(19) in our preceding Ref. [18]:

$$\hat{K}_{a,b}(\tau,\tau') = \frac{e^2}{\hbar^2}{\rm Tr}\{\hat{J}_{\beta,b}(\tau)\hat{\tau}_3\hat{G}^{+,-}_{b,a}(\tau,\tau')\hat{J}_{a,\alpha}(\tau')\hat{\tau}_3\hat{G}^{-,+}_{\alpha,\beta}(\tau',\tau) \tag{43}$$

$$+\hat{J}_{b,\beta}(\tau)\hat{\tau}_3\hat{G}^{+,-}_{\beta,\alpha}(\tau,\tau')\hat{J}_{\alpha,a}(\tau')\hat{\tau}_3\hat{G}^{-,+}_{a,b}(\tau',\tau) \tag{44}$$

$$-\hat{J}_{\beta,b}(\tau)\hat{\tau}_3\hat{G}^{+,-}_{b,\alpha}(\tau,\tau')\hat{J}_{\alpha,a}(\tau')\hat{\tau}_3\hat{G}^{-,+}_{a,\beta}(\tau',\tau) \tag{45}$$

$$-\hat{J}_{b,\beta}(\tau)\hat{\tau}_3\hat{G}^{+,-}_{\beta,a}(\tau,\tau')\hat{J}_{a,\alpha}(\tau')\hat{\tau}_3\hat{G}^{-,+}_{\alpha,b}(\tau',\tau) \tag{46}$$

$$+(\tau \leftrightarrow \tau')\}, \tag{47}$$

where $\hat{\tau}_3$ is a Pauli matrix, τ, τ' are the time variables and we assume S_a-S_c-S_b three-terminal device which is connected at the tight-binding sites a-(α,β)-b with the hopping amplitudes $J_{a,\alpha} = J_{\alpha,a}$ and $J_{b,\beta} = J_{\beta,b}$. Equations (43)–(47) can be Fourier transformed from the time variables τ, τ' to the energies $\omega + neV$ and $\omega + meV$, where n and m are two integers.

The nonvanishingly small current $I_{\rm sym} \neq 0$ of the quartets, octets or higher order clusters of Cooper pairs at the ultralong $R_0 \sim l_\varphi$ implies nonvanishingly small Keldysh Green's functions $\hat{G}^{+,-}$ and $\hat{G}^{-,+}$, see the corresponding expressions of the current in Eq. (41), (B8), and (B10)–(B13). Then, $S_{a,b} \neq 0$ at the ultralong $R_0 \sim l_\varphi$ emerges on the condition that $\hat{G}^{+,-}$ and $\hat{G}^{-,+}$ in Eqs. (43)–(47) take values in overlapping energy intervals, i.e., the bias voltage $V \neq 0$ should also be nonvanishingly small. In practice, the bias voltage energy eV is a significant fraction of the superconducting gap Δ.

Thus, within our model, the reported current $I_{\rm sym} \neq 0$ implies quantum current-noise cross-correlations $S_{a,b} \neq 0$ due to the quantum fluctuations of the current operators at the ultralong-distance $R_0 \sim l_\varphi$. Possible quantum noise cross-correlation experiments are considered now.

B. Proposed current cross-correlation experiments

On the experimental side, the positive zero-frequency quantum current-noise cross-correlations of the quartets were predicted [18] and measured in the Weizmann group experiment [31]. In this experiment, absence of the quartet line and vanishingly small quantum current-noise cross-correlations $S_{a,b} = 0$ were obtained with a pair of "remote" Josephson junctions. It was then concluded that "the trivial effect" of the electromagnetic environment is not at the origin of the quartet resonance line. The Grenoble experiment [30] also ruled out "extrinsic synchronization" by demonstrating absence of the quartet line with remote contacts in a metallic structure.

The bias voltage was very low with respect to the superconducting gap in the Weizmann group experiment [31], i.e., $eV \ll \Delta$. Here, we propose analogous measurement of the quantum current-noise cross-correlations at voltage values that are significant fractions of the gap; typically eV/Δ is within the same range as in Figs. 7–10, i.e., from $eV/\Delta = 0.3$ to $eV/\Delta = 1.2$, given the above mentioned "gap edge singularity resonance" at $eV/\Delta = 1/2$. We propose to systematically vary the distance R_0 between the junctions, in comparison with the superconducting coherence length $\xi_{\rm ball}(0)$ and the mesoscopic phase coherence length l_φ. It is expected that the ultralong-distance Floquet-Tomasch clusters of Cooper pairs are above detection threshold, given the large signal in Tomasch experiment [89–91].

VII. CONCLUSIONS

Summary of the paper and final remarks are presented now. We provided evidence for ultralong-distance nonlocality

and quantum correlations in S_a-dot-S_c-dot-S_b three-terminal Josephson junctions where the constituting S_a-dot-S_c and S_c-dot-S_b are biased at opposite voltage on the quartet line. We presented physical arguments in Sec. II and Appendix A, regarding the diagrammatic interpretation of nonlocality. Analytical theory was proposed in Secs. III and IV. We reduced the direct-gap semiconducting quantum dots to zero dimension, and demonstrated emergence of the Floquet-Andreev and Floquet-Tomasch currents limited by the relevant length scales of the superconducting coherence length $\xi_{\rm ball}(0)$ and the mesoscopic phase coherence length of the superconducting quasiparticles l_φ, respectively. The numerical calculations presented in Sec. V reveal that the ultralong-distance Floquet-Tomasch clusters of Cooper pairs emerge if the separation R_0 between the Josephson junctions exceeds the superconducting coherence length $\xi_{\rm ball}(0)$ by orders of magnitude, i.e., if $R_0 \gg \xi_{\rm ball}(0)$. This results from a phenomenological description relying on the observation that the Dynes parameter $\eta_S \ll \Delta$ is much smaller than the gap Δ, which implies that the corresponding mesoscopic phase coherence length $l_\varphi \gg \xi_{\rm ball}(0)$ of the superconducting quasiparticles is much larger than the superconducting coherence length $\xi_{\rm ball}(0)$. In addition, in agreement with the physical arguments of Sec. II, the voltage values are significant fractions of the superconducting gap Δ, typically $eV > \Delta/2n$ for a cluster of order n, where n is an integer. The typical spectral window for the ultralong-distance effect is roughly estimated as $|\omega| \approx 2\Delta$. Namely, the ultralong-distance effect is obtained and nonlocal Andreev processes are still sizable if $|\omega|$ is not large compared to the superconducting gap Δ. In this spectral window, the superconducting quasiparticles behavior reflects both the normal- and the superconducting-state properties. The numerical data confirm the expectation that increasing $R_0/\xi_{\rm ball}(0)$ from $R_0/\xi_{\rm ball}(0) \lesssim 1$ to $R_0/\xi_{\rm ball}(0) \gtrsim 1$ and to $R_0/\xi_{\rm ball}(0) \gg 1$ yields crossover from the $\sin\varphi_q$ to the $\sin(2\varphi_q)$ sensitivities of the Floquet-Andreev quartets and the ultralong-distance Floquet-Tomasch octets, respectively. Reducing eV below $\Delta/2n$ produces higher order-n clusters of Cooper pairs and dominant $\sin(n\,\varphi_q)$ harmonics in the current, where n is an integer.

The Tomasch oscillations [91] were experimentally observed with superconducting film thickness R_0 as large as $R_0 = 33.2\ \mu$m. Thus, in analogy with the Tomasch experiment [91], we conjecture emergence of the ultralong-distance Floquet-Tomasch clusters of Cooper pairs if the separation between the S_a-dot-S_c and the S_c-dot-S_b Josephson junctions is made as large as $R_0 = 33.2\ \mu$m.

This predicted ultralong-range $R_0 \sim l_\varphi$ of the Floquet-Tomasch effect is spectacularly orders of magnitude above the corresponding $R_0 \sim \xi_{\rm ball}(0)$ for overlapping Andreev bound states at $V = 0$ [23–27] or for F_aSF_b or N_aSN_b Cooper pair beam splitters, see Refs. [54–77].

Finally, we show in Appendix A that our numerical experiments on the Floquet-Tomasch clusters of Cooper pairs and the two-terminal density of state oscillations in the Tomasch experiments [89–91] both involve ultralong-distance behavior. However, the microscopic processes are different, and, in a three-terminal configuration, the coupling between the density of states at one contact and the pairs at the other contact is AC and thus, it cannot be proposed as an explanation for our numerical experiments on the DC-current of the Cooper pair clusters.

To conclude, the length scale l_φ for the mesoscopic phase coherence of the superconducting quasiparticles was phenomenologically introduced in our description. The effect offers the possibility to directly probe quantum coherence of the superconducting quasiparticle states, and to bridge with the physics of quasiparticle poisoning [6–13], in connection with the tremendous interest in the superconducting circuits of quantum engineering. It seems that future experiments could be a guideline towards further progress in understanding this complex physics. Controlling the electromagnetic environment seems to be promising for producing small values of the Dynes parameter η_S and long mesoscopic phase coherence l_φ of the superconducting quasiparticles, see Ref. [106].

ACKNOWLEDGMENTS

The author acknowledges the collaboration of the Weizmann Institute group (Y. Cohen, M. Heiblum, Y. Ronen, H. Shtrikman) on interpretation of the unpublished data which inspired this work. The author wishes to thank B. Douçot for participating to the enjoying elaboration of the framework of the interpretation. The author also thanks J.-G. Caputo and R. Danneau for discussions and critical reading of the manuscript. The author wishes to thank Ç.Ö. Girit, J.D. Pillet and their students and post-docs for sharing Refs. [23,24] prior to making their preprint publicly available. The author thanks the Centre Régional Informatique et d'Applications Numériques de Normandie (CRIANN) for the use of its facilities. The author thanks the Infrastructure de Calcul Intensif et de Données (GRICAD) for the use of the resources of the Mésocentre de Calcul Intensif de l'Université Grenoble-Alpes (CIMENT). The author acknowledges support from the French National Research Agency (ANR) in the framework of the Graphmon project (Grant No. ANR-19-CE47-0007).

APPENDIX A: CONNECTION WITH THE TOMASCH EXPERIMENT

In this Appendix, we complement the main text by drawing a parallel between the here considered nonlocal current-phase response of the Floquet-Tomasch effect, and the density of state oscillations in the Tomasch experiments [89–91]. We address this question from two points of view: the ultralong-distance nonlocality in Sec. A 1 and the structure of the electron-hole conversions in Sec. A 2. This analogy further supports the proposed interpretation of the numerical experiments in terms of the diagrams that capture nonlocality, see Sec. II. We justify in Sec. A 2 the use of the vocabulary "the Floquet-Tomasch effect" for the current of pairs in a three-terminal Josephson junction. We also conclude to different quantum processes in the density of state oscillations of the Tomasch effect [89–91] and the current of pairs in a three-terminal Josephson junction. Thus the former cannot be used to explain our calculations on the latter.

1. Effects of a boundary

In this section, we start from a superconductor with open boundary conditions, according to Wolfram and Lehman in

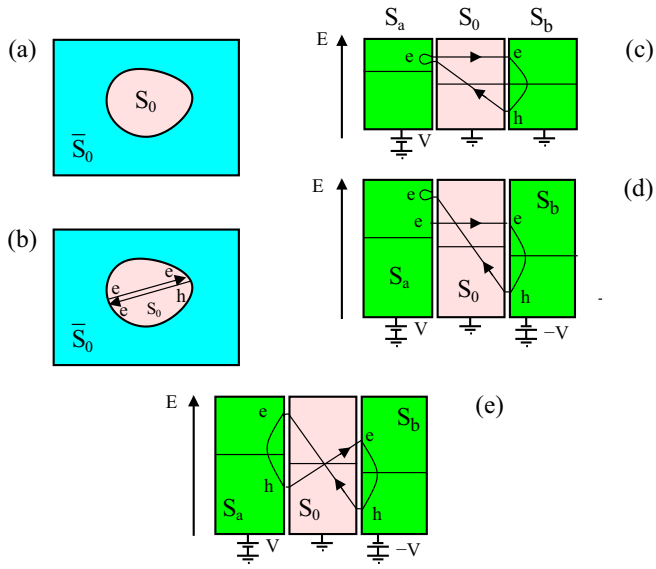

FIG. 11. (a) shows how a finite-size superconductor is defined in a bulk 3D superconductor, S_0 and $\overline{S}_0$ being the interior and the exterior, respectively. (b) shows nonlocality and a schematic representation of Eq. (6) in Ref. [92]. (c) shows the "triangular energy diagram" for the DC-local density of states in a two-terminal configuration, as in the Tomasch experiment [89–91]. (d) shows the AC density of states in a three-terminal configuration, where S_a and S_b are biased at opposite voltage while S_0 is grounded. (e) shows the three-terminal "butterfly quartet energy diagram" for the DC transport of pairs and the Floquet-Tomasch effect, see also Fig. 3.

Ref. [93], and demonstrate that this implies nonlocality in the sense of Eq. (6) in Ref. [92] by McMillan and Anderson.

Namely, we consider that a finite-size region S_0 is defined in an infinite 3D superconductor. The "interior" and the "exterior" are denoted by S_0 an $\overline{S}_0$, respectively. Thus $S_0 + \overline{S}_0$ is an infinite 3D superconductor, see Fig. 11(a).

We assume that the two-dimensional (2D) surface of S_0 is practically realized with a collection of the Nambu hopping amplitudes denoted by $\Sigma_{S_0,\overline{S}_0}$ and $\Sigma_{\overline{S}_0,S_0}$ for hopping between S_0 and $\overline{S}_0$ and between $\overline{S}_0$ and S_0 respectively. Those matrices $\Sigma_{S_0,\overline{S}_0}$ and $\Sigma_{\overline{S}_0,S_0}$ have entries in the tight-binding sites making the S_0-$\overline{S}_0$ interface and in the Nambu labels (i.e., they are diagonal in the Nambu labels).

We denote by g and G the Green's functions of $S_0 + \overline{S}_0$ and S_0 respectively. We obtain G for S_0 by including the hopping self-energies $\tilde{\Sigma}_{S_0,\overline{S}_0} = -\Sigma_{S_0,\overline{S}_0}$ and $\tilde{\Sigma}_{\overline{S}_0,S_0} = -\Sigma_{\overline{S}_0,S_0}$, which cancel the plain 3D tight-binding amplitudes on the S_0-$\overline{S}_0$ boundary. Thus S_0 is disconnected from $\overline{S}_0$ in the Green' function G which is fully dressed with the self-energy $\tilde{\Sigma}$.

The Dyson equations

$$\left(I - g_{S_0,\overline{S}_0}\tilde{\Sigma}_{\overline{S}_0,S_0}\right)G_{S_0,S_0} - g_{S_0,S_0}\tilde{\Sigma}_{S_0,\overline{S}_0}G_{\overline{S}_0,S_0} = g_{S_0,S_0} \quad \text{(A1)}$$

$$-g_{\overline{S}_0,\overline{S}_0}\tilde{\Sigma}_{\overline{S}_0,S_0}G_{S_0,S_0} + \left(I - g_{\overline{S}_0,S_0}\tilde{\Sigma}_{S_0,\overline{S}_0}\right)G_{\overline{S}_0,S_0} = g_{\overline{S}_0,S_0} \quad \text{(A2)}$$

have the following solution:

$$G_{S_0,S_0} = \left[I - g_{\overline{S}_0,\overline{S}_0}\tilde{\Sigma}_{\overline{S}_0,S_0} - g_{S_0,S_0}\tilde{\Sigma}_{S_0,\overline{S}_0}\left(I - g_{\overline{S}_0,S_0}\tilde{\Sigma}_{S_0,\overline{S}_0}\right)^{-1}g_{\overline{S}_0,\overline{S}_0}\tilde{\Sigma}_{\overline{S}_0,S_0}\right]^{-1} \times \left[g_{S_0,S_0} + g_{S_0,S_0}\tilde{\Sigma}_{S_0,\overline{S}_0}\left(I - g_{\overline{S}_0,S_0}\tilde{\Sigma}_{S_0,\overline{S}_0}\right)^{-1}g_{\overline{S}_0,S_0}\right]. \quad \text{(A3)}$$

The density of states is sometimes called as "the local density of states" because it can be measured with a local probe. It turns out that the density of states in the Tomasch experiment nonlocally couples to all of the thin-film boundary, if the conditions are met, regarding the characteristic energy and length scales. Specifically, we consider $R_0 \lesssim l_\varphi$, where R_0 is the linear dimension of S_0, see Figs. 11(a) and 11(b). In addition, we assume that the energy is in the range $|\omega| \approx 2\Delta$, see the discussion in Sec. III B. The phenomenological mesoscopic phase coherence length l_φ was introduced above in Sec. III. Then, Eq. (A3) implies that all pairs of tight-binding sites at the boundary of S_0 are connected to each other by the matrix G_{S_0,S_0} taking roughly similar order of magnitude for all pairs of sites at the boundary, on the conditions $R_0 \lesssim l_\varphi$ and $\omega \approx 2\Delta$.

Equation (A3) also implies that conversion of spin-up electron into spin-down hole (and vice versa) is effective at the boundary of S_0, which directly leads to Eq. (6) in Ref. [92], see also Fig. 11(b). This implies compatibility of our diagrammatic description with both Refs. [92,93].

2. The corresponding diagrams

Now, we consider the electron-hole Nambu labels and examine a single framework for deducing the different quantum processes that lead to the Tomasch density of states oscillations [89–91] and to the Floquet-Tomasch pair current in three-terminal Josephson junctions. Those quantum processes are characterized by the distinct diagrams in Figs. 11(c)–11(e).

Equation (6) in Ref. [92] can schematically be represented by the two-terminal "triangular diagram" in Fig. 11(c). This quantum process involves Andreev reflection at the thin-film boundary in the sense of spin-up electron quasiparticle from S_0 being reflected as spin-down hole quasiparticle in S_0. Then, a pair transmitted from the quasiparticles states into the condensate of the same S_0, and the crystal lattice has to be free to move in order to absorb the recoil coming from conservation of momentum. The diagram in Fig. 11(c) involves electron-electron propagation in the left superconductors S_a and electron-hole conversion in the right superconductor S_b. Thus Fig. 11(c) encodes the Tomasch effect in the sense Ref. [92], i.e., the variations of the density of states at the left interface as a function of the electron-hole conversion at the other contact.

Conversely, Fig. 11(d) shows schematically the three-terminal diagram for the density of states. It does not form a loop and thus, in a three-terminal configuration, the response in the density of states at one contact in S_a as a function of the pair amplitude in S_c features AC oscillations.

Finally, the current of pairs in a double Josephson junction biased at opposite voltages is captured by the "quartet butterfly energy diagram" in Fig. 11(e), see also Ref. [14] and Figs. 3(a) and 3(b) in Sec. II. In Fig. 11(e), two pairs are taken from S_0, they exchange partners, a pair is transmitted into the left superconductors S_a in the final state, and another one into S_b according to the quartet process [14].

Thus, energy conservation implies that the "triangular diagram process" in Fig. 11(c) is DC in the two-terminal configuration of the Tomasch experiment [89–91], but it becomes AC in the three-terminal Josephson biased at opposite voltage. By contrast the quartet diagram in Fig. 11(e) is DC and this is why our numerical calculations for the DC-ultralong-distance Floquet-Tomasch current of pairs cannot be interpreted in terms of the AC density of state. Instead, they naturally receive the proposed interpretation of the quartets and higher order clusters of Cooper pairs.

However, the straightforward wording of "the Floquet-Tomasch effect" is used throughout the paper for the three-terminal Josephson junction, in order to refer to the common origin of the ultralong-distance coupling in both cases.

APPENDIX B: DETAILS ON THE METHODS

This section summarizes the method to evaluate the currents. The calculation of the current [98,100] starts with expression of the bare advanced and retarded Green's functions.

The bare Green's function of each quantum dot is given by $g_{\rm dot}(\omega) = (\omega - \mathscr{H}_{\rm dot} - i\eta)^{-1}$, where ω is the energy and $\mathscr{H}_{\rm dot}$ is the quantum dot Hamiltonian. Assuming the energy levels ε_α and the wave functions $\langle \mathbf{x}|\alpha\rangle$ (at the location $\mathbf{x}$) yields the following electron-electron Green's function between $\mathbf{x}$ and $\mathbf{y}$:

$$g^A_{\mathbf{x},\mathbf{y}}(\omega) = \sum_\alpha \langle \mathbf{x}|\alpha\rangle \frac{1}{\omega - \varepsilon_\alpha - \varepsilon_g - i\eta} \langle \alpha|\mathbf{y}\,\rangle, \tag{B1}$$

where the gate voltage V_g-tunable energy ε_g fulfills the condition $\varepsilon_{\alpha_0} + \varepsilon_g = 0$ if $\alpha = \alpha_0$, yielding resonance at zero energy $\omega = 0$ (see Fig. 1 for the gates). Then, $g^A_{\mathbf{x},\mathbf{y}}(\omega)$ is Eq. (B1) is approximated as

$$g^A_{\mathbf{x},\mathbf{y}}(\omega) \simeq \frac{1}{\omega - i\eta} \langle \mathbf{x}|\alpha_0\rangle \langle \alpha_0|\mathbf{y}\,\rangle. \tag{B2}$$

The parameter η in Eq. (B1) is related to the strength of relaxation. It was found in Ref. [17] that tiny relaxation $0 < \eta \ll \Delta$ has huge effect on the quartet current, in comparison with the previous Ref. [16] where $\eta = 0^+$. However, the available experimental data [31] do not allow to demonstrate that $0 < \eta \ll \Delta$ in Ref. [17] is more relevant than $\eta = 0^+$ in Ref. [16]. This is why the approximation $\eta = 0^+$ is used in absence of further experimental input.

The 2×2 Nambu representation has entries for spin-up electrons and spin-down holes:

$$\hat{g}^A_{\mathbf{x},\mathbf{y}}(t,t') = -i\theta(t-t') \begin{pmatrix} \langle\{c_{\mathbf{x},\uparrow}(t), c^+_{\mathbf{y},\uparrow}(t')\}\rangle & \langle\{c_{\mathbf{x},\uparrow}(t), c_{\mathbf{y},\downarrow}(t')\}\rangle \\ \langle\{c^+_{\mathbf{x},\downarrow}(t), c^+_{\mathbf{y},\uparrow}(t')\}\rangle & \langle\{c^+_{\mathbf{x},\downarrow}(t), c_{\mathbf{y},\downarrow}(t')\}\rangle \end{pmatrix}, \tag{B3}$$

where $\langle\rangle$ denotes averaging in the stationary state, $\{\}$ is an anticommutator, $\mathbf{x}$, $\mathbf{y}$ are the space coordinates and t, t' are the time variables.

Using Eq. (B3) and the Hamiltonian given by Eqs. (4) and (5), we find the expression of the bare superconducting Green's function with gap Δ and phase φ:

$$\hat{g}^A_{\mathbf{x},\mathbf{y}}(\omega) = \frac{1}{W}\frac{1}{k_F R} \exp\left\{\left(-\frac{R}{\xi_{\rm ball}(\omega - i\eta_S)}\right)\right\}\left[\frac{\cos\psi_F}{\sqrt{\Delta^2 - (\omega - i\eta_S)^2}} \begin{pmatrix} -(\omega - i\eta_S) & \Delta e^{i\varphi} \\ \Delta e^{-i\varphi} & -(\omega - i\eta_S) \end{pmatrix} + \sin\psi_F \begin{pmatrix} -1 & 0 \\ 0 & 1 \end{pmatrix}\right], \tag{B4}$$

where $R = |\mathbf{x} - \mathbf{y}|$ is the distance between $\mathbf{x}$ and $\mathbf{y}$ and $\varphi = \varphi_a$, φ_b, φ_c according to which of the S_a, S_b or S_c superconducting lead is considered. The phase $\psi_F = k_F R$ in Eq. (B4) oscillates at the scale of the small Fermi wave-length $\lambda_F = 2\pi/k_F$, where k_F is the Fermi wave vector. The ballistic superconducting coherence length $\xi_{\rm ball}$ at the energy ω is given by Eq. (3).

Considering first vanishingly small bias voltage $V = 0$, the Nambu hopping amplitude connecting each quantum dot to the superconductors takes the form

$$\hat{J} = \begin{pmatrix} J_0 & 0 \\ 0 & -J_0 \end{pmatrix}, \tag{B5}$$

where each contact has different J_0. For instance $J_0 \equiv J_{a,\alpha}$ at the a-α interface on Fig. 5, and $J_0 \equiv J_{c,\gamma}$, $J_{c',\gamma'}$ and $J_{b,\beta}$ at the c-γ, c'-γ' and b-β interfaces.

The fully dressed advanced and retarded Nambu Green's functions $\hat{G}^{A,R}$ are deduced from the bare ones by use of the Dyson equation

$$\hat{G}^{A,R} = \hat{g}^{A,R} + \hat{g}^{A,R} \otimes \hat{J} \otimes \hat{G}^{A,R}, \tag{B6}$$

where $\otimes$ denotes convolution over the time variables and summation over the specific tight-binding sites at both ends of the tunneling amplitude $\hat{J}$ connecting the dots to the superconductors.

Assuming now voltage biasing on the quartet line according to Eq. (1), the superconducting phases $\varphi_a(t)$, $\varphi_b(t)$ and $\varphi_c(t)$ of S_a, S_b and S_c evolve according to the Josephson relations mentioned in the Introduction. The overall quantum dynamics being time-periodic, the Fourier-transformed Nambu Green's functions acquire the integer labels n, m regarding the harmonics $(2neV/\hbar, 2meV/\hbar)$ of the frequency $2eV/\hbar$ associated to the voltage V.

The fully dressed Keldysh Green's function $\hat{G}^{+,-}$ is given by [98,100]

$$\hat{G}^{+,-} = (\hat{I} + \hat{G}^R \otimes \hat{J}) \otimes \hat{g}^{+,-} \otimes (\hat{I} + \hat{J} \otimes \hat{G}^A), \quad \text{(B7)}$$

where the bare Keldysh Green's function is $\hat{g}^{+,-}(\omega) = n_F(\omega)[\hat{g}^A(\omega) - \hat{g}^R(\omega)]$, with $n_F(\omega)$ the Fermi-Dirac distribution function i.e., $n_F(\omega) = \theta(-\omega)$ in the limit of zero temperature, with $\theta(x) = 1$ if $x > 0$ and $\theta(x) = 0$ if $x < 0$.

The current is next deduced from $\hat{G}^{+,-}$ given by Eq. (B7). For instance, the current through the $a - \alpha$ interface at time t is given by [98,100]

$$I_{a-\alpha}(t) = \frac{2e}{\hbar} \sum_p \left[\hat{J}_{\alpha_p,a_p} \hat{G}^{+,-}_{a_p,\,\alpha_p}(t,t) - \hat{J}_{a_p,\,\alpha_p} \hat{G}^{+,-}_{\alpha_p,a_p}(t,t)\right]_{(1,1)}. \quad \text{(B8)}$$

The subscript "(1, 1)" in Eq. (B8) stands for the electron-electron Nambu component. Eq. (B8) can be expressed as

$$I_{a-\alpha} = \frac{e}{\hbar} \int \mathscr{I}_{a,\alpha}(\omega) d\omega, \quad \text{(B9)}$$

where the spectral current takes the form

$$\mathscr{I}_{a,\alpha}(\omega) = \sum_p \Big[\big(\hat{J}_{\alpha_p,a_p} \hat{G}^{+,-}_{a_p,\,\alpha_p}\big)_{(1,1)/(0,0)}(\omega) \quad \text{(B10)}$$

$$- \big(\hat{J}_{\alpha_p,a_p} \hat{G}^{+,-}_{a_p,\,\alpha_p}\big)_{(2,2)/(0,0)}(\omega) \quad \text{(B11)}$$

$$- \big(\hat{J}_{a_p,\alpha_p} \hat{G}^{+,-}_{\alpha_p,\,a_p}\big)_{(1,1)/(0,0)}(\omega) \quad \text{(B12)}$$

$$+ \big(\hat{J}_{a_p,\alpha_p} \hat{G}^{+,-}_{\alpha_p,\,a_p}\big)_{(2,2)/(0,0)}(\omega)\Big]. \quad \text{(B13)}$$

The subscripts "(1,1)" and "(2,2)" correspond to the "electron-electron" and "hole-hole" Nambu components and "(0,0)" encodes $n = m = 0$ in the $(neV/\hbar, meV/\hbar)$ labels of the harmonics of the Josephson frequency.

APPENDIX C: DETAILS ON THE ANALYTICAL CALCULATIONS

Combining the Dyson Eq. (B6) to Eqs. (19) and (20) yields

$$G_{\alpha,\,\alpha} = \tilde{g}_{\alpha,x} \tilde{G}_{x,x} \tilde{g}_{x,\,\alpha}, \quad \text{(C1)}$$

$$G_{\gamma,\,\alpha} = \tilde{g}_{\gamma,x} \tilde{G}_{x,x} \tilde{g}_{x,\,\alpha}. \quad \text{(C2)}$$

The Dyson equations take the form

$$G_{\alpha,\,\alpha} = g_{\alpha,\,\alpha} + g_{\alpha,\,\alpha} \Sigma_{\alpha,a} g_{a,a} \Sigma_{a,\,\alpha} G_{\alpha,\,\alpha} + g_{\alpha,\,\gamma} \Sigma_{\gamma,c} g_{c,c} \Sigma_{c,\,\gamma} G_{\gamma,\,\alpha} + g_{\alpha,\,\gamma} \Sigma_{\gamma,c} g_{c,c'} \Sigma_{c',\,\gamma'} G_{\gamma',\,\alpha}, \quad \text{(C3)}$$

$$G_{\gamma,\,\alpha} = g_{\gamma,\,\alpha} + g_{\gamma,\,\alpha} \Sigma_{\alpha,a} g_{a,a} \Sigma_{a,\,\alpha} G_{\alpha,\,\alpha} + g_{\gamma,\,\gamma} \Sigma_{\gamma,c} g_{c,c} \Sigma_{c,\,\gamma} G_{\gamma,\,\alpha} + g_{\gamma,\,\gamma} \Sigma_{\gamma,c} g_{c,c'} \Sigma_{c',\,\gamma'} G_{\gamma',\,\alpha}. \quad \text{(C4)}$$

Then, Eqs. (C1)–(C2) and (C3) yield

$$\tilde{G}_{x,x} = \tilde{g}_{x,x} + \tilde{g}_{x,x} \tilde{K}_{x,x} \tilde{G}_{x,x} + \tilde{g}_{x,x} \tilde{K}_{x,x'} \tilde{G}_{x',x}, \quad \text{(C5)}$$

where

$$\tilde{K}_{x,x} = \tilde{g}_{x,\,\alpha} \Sigma_{\alpha,a} g_{a,a} \Sigma_{a,\,\alpha} g_{\alpha,x} + \tilde{g}_{x,\,\gamma} \Sigma_{\gamma,c} g_{c,c} \Sigma_{c,\,\gamma} \tilde{g}_{\gamma,x}, \quad \text{(C6)}$$

$$\tilde{K}_{x,x'} = \tilde{g}_{x,\,\gamma} \Sigma_{\gamma,c} g_{c,c'} \Sigma_{c',\,\gamma'} \tilde{g}_{\gamma',x'}. \quad \text{(C7)}$$

Conversely, Eqs. (C1)–(C2) and (C4) yield

$$\tilde{G}_{x,x} = \tilde{g}_{x,x} + \tilde{g}_{x,x} \tilde{K}'_{x,x} \tilde{G}_{x,x} + \tilde{g}_{x,x} + \tilde{g}_{x,x} \tilde{K}'_{x,x'} \tilde{G}_{x',x}, \quad \text{(C8)}$$

where it turns out that $\tilde{K}'_{x,x} = \tilde{K}_{x,x}$ and $\tilde{K}'_{x,x'} = \tilde{K}_{x,x'}$. Thus Eqs. (C5) and (C8) are compatible with each other. Given Eq. (B7), (B10)–(B13), and (C1), we obtain

$$\Sigma_{a,\,\alpha} G^{+,-}_{\alpha,a} \quad \text{(C9)}$$

$$= (\Sigma_{a,\,\alpha} \tilde{g}_{\alpha,x} \tilde{G}_{x,x} \tilde{g}_{x,x} \Sigma_{\alpha,a} g_{a,a})^{+,-} \quad \text{(C10)}$$

$$= \Sigma_{a,\,\alpha} \tilde{g}^{+,-}_{\alpha,x} \tilde{G}^A_{x,x} \tilde{g}^A_{x,x} \Sigma_{\alpha,a} g^A_{a,a} \quad \text{(C11)}$$

$$+ \Sigma_{a,\,\alpha} \tilde{g}^R_{\alpha,x} \tilde{G}^{+,-}_{x,x} \tilde{g}^A_{x,x} \Sigma_{\alpha,a} g^A_{a,a} \quad \text{(C12)}$$

$$+ \Sigma_{a,\,\alpha} \tilde{g}^R_{\alpha,x} \tilde{G}^R_{x,x} \tilde{g}^{+,-}_{x,x} \Sigma_{\alpha,a} g^A_{a,a} \quad \text{(C13)}$$

$$+ \Sigma_{a,\,\alpha} \tilde{g}^R_{\alpha,x} \tilde{G}^R_{x,x} \tilde{g}^R_{x,x} \Sigma_{\alpha,a} g^{+,-}_{a,a}. \quad \text{(C14)}$$

The Dyson Eqs. (C3) and (C4)

$$\tilde{G}_{x,x} = \tilde{g}_{x,x} + \tilde{g}_{x,x} \tilde{K}_{x,x} \tilde{G}_{x,x} + \tilde{g}_{x,x} \tilde{K}_{x,x'} \tilde{G}_{x',x}, \quad \text{(C15)}$$

$$\tilde{G}_{x',x} = \tilde{g}_{x',x'} \tilde{K}_{x',x} \tilde{G}_{x,x} + \tilde{g}_{x',x'} \tilde{K}_{x',x'} \tilde{G}_{x',x} \quad \text{(C16)}$$

lead to

$$\tilde{G}_{x,x} = [I - \tilde{L}_{x,x} \tilde{K}_{x,x'} \tilde{L}_{x',x'} \tilde{K}_{x',x}]^{-1} \tilde{L}_{x,x}, \quad \text{(C17)}$$

where

$$\tilde{L}_{x,x} = [(\tilde{g}_{x,x})^{-1} - \tilde{K}_{x,x}]^{-1}, \quad \text{(C18)}$$

$$\tilde{L}_{x',x'} = [(\tilde{g}_{x',x'})^{-1} - \tilde{K}_{x',x'}]^{-1}. \quad \text{(C19)}$$

Then, we deduce Eqs. (21)–(24) in Sec. IV.

[1] D. Kouznetsov, D. Rohrlich, and R. Ortega, Quantum limit of noise of a phase-invariant amplifier, Phys. Rev. A **52**, 1665 (1995).

[2] *The SQUID Handbook: Applications of SQUIDs and SQUID Systems*, edited by J. Clarke, and A. I. Braginski (John Wiley & Sons, Ltd, 2004).

[3] J. Clarke, and F. K. Wilhelm, Superconducting quantum bits, Nature (London) **453**, 1031 (2008).

[4] M. H. Devoret and R. J. Schoelkopf, Superconducting circuits for quantum information: An outlook, Science **339**, 1169 (2013).

[5] F. Arute *et al.*, Quantum supremacy using a programmable superconducting processor, Nature (London) **574**, 505 (2019).

[6] J. M. Martinis, M. Ansmann, and J. Aumentado, Energy Decay in Superconducting Josephson-Junction Qubits from Nonequilibrium Quasiparticle Excitations, Phys. Rev. Lett. **103**, 097002 (2009).

[7] P. J. de Visser, J. J. A. Baselmans, P. Diener, S. J. C. Yates, A. Endo, and T. M. Klapwijk, Number Fluctuations of Sparse Quasiparticles in a Superconductor, Phys. Rev. Lett. **106**, 167004 (2011).

[8] M. Lenander, H. Wang, R. C. Bialczak, E. Lucero, M. Mariantoni, M. Neeley, A. D. O'Connell, D. Sank, M. Weides, J. Wenner, T. Yamamoto, Y. Yin, J. Zhao, A. N. Cleland, and J. M. Martinis, Measurement of energy decay in superconducting qubits from nonequilibrium quasiparticles, Phys. Rev. B **84**, 024501 (2011).

[9] S. Rajauria, L. M. A. Pascal, Ph. Gandit, F. W. J. Hekking, B. Pannetier, and H. Courtois, Efficiency of quasiparticle evacuation in superconducting devices, Phys. Rev. B **85**, 020505(R) (2012).

[10] J. Wenner, Y. Yin, E. Lucero, R. Barends, Y. Chen, B. Chiaro, J. Kelly, M. Lenander, M. Mariantoni, A. Megrant, C. Neill, P. J. J. O'Malley, D. Sank, A. Vainsencher, H. Wang, T. C. White, A. N. Cleland, and J. M. Martinis, Excitation of Superconducting Qubits from Hot Nonequilibrium Quasiparticles, Phys. Rev. Lett. **110**, 150502 (2013).

[11] D. Ristè, C. C. Bultink, M. J. Tiggelman, R. N. Schouten, K. W. Lehnert, L. DiCarlo, Millisecond charge-parity fluctuations and induced decoherence in a superconducting transmon qubit, Nat. Commun. **4**, 1913 (2013).

[12] E. M. Levenson-Falk, F. Kos, R. Vijay, L. Glazman, and I. Siddiqi, Single-Quasiparticle Trapping in Aluminum Nanobridge Josephson Junctions, Phys. Rev. Lett. **112**, 047002 (2014).

[13] J. S. Meyer, M. Houzet and A. V. Nazarov, Dynamical Spin Polarization of Excess Quasi-Particles in Superconductors, Phys. Rev. Lett. **125**, 097006 (2020).

[14] A. Freyn, B. Douçot, D. Feinberg, and R. Mélin, Production of Non-Local Quartets and Phase-Sensitive Entanglement in a Superconducting Beam Splitter, Phys. Rev. Lett. **106**, 257005 (2011).

[15] R. Mélin, D. Feinberg, and B. Douçot, Partially resummed perturbation theory for multiple Andreev reflections in a short three-terminal Josephson junction, Eur. Phys. J. B **89**, 67 (2016).

[16] T. Jonckheere, J. Rech, T. Martin, B. Douçot, D. Feinberg, and R. Mélin, Multipair DC Josephson resonances in a biased all-superconducting bijunction, Phys. Rev. B **87**, 214501 (2013).

[17] R. Mélin, J.-G. Caputo, K. Yang and B. Douçot, Simple Floquet-Wannier-Stark-Andreev viewpoint and emergence of low-energy scales in a voltage-biased three-terminal Josephson junction, Phys. Rev. B **95**, 085415 (2017).

[18] R. Mélin, M. Sotto, D. Feinberg, J.-G. Caputo and B. Douçot, Gate-tunable zero-frequency current cross-correlations of the quartet mode in a voltage-biased three-terminal Josephson junction, Phys. Rev. B **93**, 115436 (2016).

[19] R. Mélin, R. Danneau, K. Yang, J.-G. Caputo, and B. Douçot, Engineering the Floquet spectrum of superconducting multiterminal quantum dots, Phys. Rev. B **100**, 035450 (2019).

[20] R. Mélin and B. Douçot, Inversion in a four terminal superconducting device on the quartet line. I. Two-dimensional metal and the quartet beam splitter, Phys. Rev. B **102**, 245435 (2020).

[21] R. Mélin and B. Douçot, Inversion in a four terminal superconducting device on the quartet line. II. Quantum dot and Floquet theory, Phys. Rev. B **102**, 245436 (2020).

[22] R. Mélin, The dc-Josephson effect with more than four superconducting leads, arXiv:2103.03519 v1.

[23] J. D. Pillet, V. Benzoni, J. Griesmar, J.-L. Smirr, and Ç. Ö. Girit, Nonlocal Josephson effect in Andreev molecules Nano Lett. **19**, 7138 (2019).

[24] J.-D. Pillet, V. Benzoni, J. Griesmar, J.-L. Smirr, and Ç. Ö. Girit, Scattering description of Andreev molecules, SciPost Phys. Core **2**, 009 (2020).

[25] Z. Scherübl, A. Pályl and S. Csonka, Transport signatures of an Andreev molecule in a quantum dot-superconductor-quantum dot setup, Beilstein J. Nanotechnol. **10**, 363 (2019).

[26] V. Kornich, H. S. Barakov, and Yu. V. Nazarov, Fine energy splitting of overlapping Andreev bound states in multiterminal superconducting nanostructures, Phys. Rev. Res. **1**, 033004 (2019).

[27] V. Kornich, H. S. Barakov and Yu. V. Nazarov, Overlapping Andreev states in semiconducting nanowires: Competition of 1D and 3D propagation, Phys. Rev. B **101**, 195430 (2020).

[28] H.-Y. Xie, M. G. Vavilov and A. Levchenko, Topological Andreev bands in three-terminal Josephson junctions, Phys. Rev. B **96**, 161406(R) (2017).

[29] H.-Y. Xie, M. G. Vavilov and A. Levchenko, Weyl nodes in Andreev spectra of multiterminal Josephson junctions: Chern numbers, conductances and supercurrents, Phys. Rev. B **97**, 035443 (2018).

[30] A. H. Pfeffer, J. E. Duvauchelle, H. Courtois, R. Mélin, D. Feinberg, and F. Lefloch, Subgap structure in the conductance of a three-terminal Josephson junction, Phys. Rev. B **90**, 075401 (2014).

[31] Y. Cohen, Y. Ronen, J. H. Kang, M. Heiblum, D. Feinberg, R. Mélin, and H. Strikman, Non-local supercurrent of quartets in a three-terminal Josephson junction, Proc. Natl. Acad. Sci. USA **115**, 6991 (2018).

[32] K. F. Huang, Y. Ronen, R. Mélin, D. Feinberg, K. Watanabe, T. Taniguchi, and P. Kim, Quartet supercurrent in a multi-terminal Graphene-based Josephson Junction, arXiv:2008.03419.

[33] E. Strambini, S. D'Ambrosio, F. Vischi, F. S. Bergeret, Yu. V. Nazarov, and F. Giazotto, The ω-SQUIPT as a tool to phase-engineer Josephson topological materials, Nat. Nanotechnol. **11**, 1055 (2016).

[34] A. W. Draelos, M.-T. Wei, A. Seredinski, H. Li, Y. Mehta, K. Watanabe, T. Taniguchi, I. V. Borzenets, F. Amet, and G. Finkelstein, Supercurrent flow in multiterminal graphene Josephson junctions, Nano Lett. **19**, 1039 (2019).

[35] N. Pankratova, H. Lee, R. Kuzmin, K. Wickramasinghe, W. Mayer, J. Yuan, M. Vavilov, J. Shabani and V. Manucharyan, The Multi-Terminal Josephson Effect, Physical Review X **10**, 031051 (2020).

[36] G. V. Graziano, J. S. Lee, M. Pendharkar, C. Palmstrom and V. S. Pribiag, Transport Studies in a Gate-Tunable Three-Terminal Josephson Junction, Phys. Rev. B **101**, 054510 (2020).

[37] E. G. Arnault, T. Larson, A. Seredinski, L. Zhao, H. Li, K. Watanabe, T. Tanniguchi, I. Borzenets, F. Amet and G. Finkelstein, The multiterminal inverse AC Josephson effect, arXiv:2012.15253 v1.

[38] S. A. Khan, L. Stampfer, T. Mutas, J.-H. Kang, P. Krogstrup and T. S. Jespersen, Multiterminal Quantized Conductance in InSb Nanocrosses, arXiv:2101.02529.

[39] O. Kürtössy, Z. Scherübl, G. Fülöp, I. E. Lukács, T. Kanne, J. Nygard, P. Makk and S. Csonka, Andreev molecule in parallel InAs nanowires, arXiv:2103.14083.
[40] R.-P. Riwar, M. Houzet, J. S. Meyer, and Y. V. Nazarov, Multi-terminal Josephson junctions as topological materials, Nat. Commun. **7**, 11167 (2016).
[41] E. Eriksson, R.-P. Riwar, M. Houzet, J. S. Meyer, and Y. V. Nazarov, Topological transconductance quantization in a four-terminal Josephson junction, Phys. Rev. B **95**, 075417 (2017).
[42] O. Deb, K. Sengupta and D. Sen, Josephson junctions of multiple superconducting wires, Phys. Rev. B **97**, 174518 (2018).
[43] H. Weisbrich, R. L. Klees, G. Rastelli and W. Belzig, Second chern number and non-Abelian berry phase in topological superconducting systems, PRX Quantum **2**, 010310 (2021).
[44] V. Fatem, A. R. Akhmerov and L. Bretheau, Weyl Josepshon circuits, Phys. Rev. Research **3**, 013288 (2021).
[45] L. Peyruchat, J. Griesmar, J.-D. Pillet and Ç. Ö. Girit, Transconductance quantization in a topological Josephson tunnel junction circuit, Phys. Rev. Research **3**, 013289 (2021).
[46] Y. Chen and Y. V. Nazarov, Weyl point immersed in a continuous spectrum: An example from superconducting nanostructures, arXiv:2102.03947 v1.
[47] E. V. Repin and Y. V. Nazarov, Weyl points in the multi-terminal Hybrid Superconductor-Semiconductor Nanowire devices, arXiv:2010.11494 v1.
[48] B. Douçot, R. Danneau, K. Yang, J.-G. Caputo and R. Mélin, Berry phase in superconducting multiterminal quantum dots, Phys. Rev. B **101**, 035411 (2020).
[49] B. Venitucci, D. Feinberg, R. Mélin, B. Douçot, Nonadiabatic Josephson current pumping by microwave irradiation, Phys. Rev. B **97**, 195423 (2018).
[50] L. P. Gavensky, G. Usaj, D. Feinberg and C. A. Balseiro, Berry curvature tomography and realization of topological Haldane model in driven three-terminal Josephson junctions, Phys. Rev. B **97**, 220505(R) (2018).
[51] R. L. Klees, G. Rastelli, J. C. Cuevas, and W. Belzig, Microwave Spectroscopy Reveals the Quantum Geometric Tensor of Topological Josephson Matter, Phys. Rev. Lett. **124**, 197002 (2020).
[52] M. A. H. Nerenberg, J. A. Blackburn, and D. W. Jillie, Voltage locking and other interactions in coupled superconducting weak links. I. Theory, Phys. Rev. B **21**, 118 (1980).
[53] D. W. Jillie, M. A. H. Nerenberg, and J. A. Blackburn, Voltage locking and other interactions in coupled superconducting weak links. II. Experiment, Phys. Rev. B **21**, 125 (1980).
[54] D. Beckmann, H. B. Weber, and H.v. Löhneysen, Evidence for Crossed Andreev Reflection in Superconductor-Ferromagnet Hybrid Structures, Phys. Rev. Lett. **93**, 197003 (2004).
[55] S. Russo, M. Kroug, T. M. Klapwijk, and A. F. Morpurgo, Experimental Observation of Bias-Dependent Nonlocal Andreev Reflection, Phys. Rev. Lett. **95**, 027002 (2005).
[56] P. Cadden-Zimansky and V. Chandrasekhar, Nonlocal Correlations in Normal-Metal Superconducting Systems, Phys. Rev. Lett. **97**, 237003 (2006).
[57] P. Cadden-Zimansky, Z. Jiang, and V. Chandrasekhar, Charge imbalance, crossed Andreev reflection and elastic co-tunneling in ferromagnet/superconductor/normal-metal structures, New J. Phys. **9**, 116 (2007).
[58] L. G. Herrmann, F. Portier, P. Roche, A. Levy Yeyati, T. Kontos, and C. Strunk, Carbon Nanotubes as Cooper Pair Beam Splitters, Phys. Rev. Lett. **104**, 026801 (2010).
[59] L. Hofstetter, S. Csonka, J. Nygoard, and C. Schönenberger, Cooper pair splitter realized in a two-quantum-dot Y-junction, Nature (London) **461**, 960 (2009).
[60] J. Wei and V. Chandrasekhar, Positive noise cross-correlation in hybrid superconducting and normal-metal three-terminal devices, Nat. Phys. **6**, 494 (2010).
[61] A. Das, Y. Ronen, M. Heiblum, D. Mahalu, A. V. Kretinin, and H. Shtrikman, High-efficiency Cooper pair splitting demonstrated by two-particle conductance resonance and positive noise cross- correlation, Nat. Commun. **3**, 1165 (2012).
[62] M. S. Choi, C. Bruder, and D. Loss, Spin-dependent Josephson current through double quantum dots and measurement of entangled electron states, Phys. Rev. B **62**, 13569 (2000).
[63] P. Recher, E. V. Sukhorukov, and D. Loss, Andreev tunneling, Coulomb blockade, and resonant transport of nonlocal spin-entangled electrons, Phys. Rev. B **63**, 165314 (2001).
[64] G. B. Lesovik, T. Martin, and G. Blatter, Electronic entanglement in the vicinity of a superconductor, Eur. Phys. J. B **24**, 287 (2001).
[65] N. M. Chtchelkatchev, G. Blatter, G. B. Lesovik, and T. Martin, Bell inequalities and entanglement in solid-state devices, Phys. Rev. B **66**, 161320(R) (2002).
[66] A. V. Lebedev, G. B. Lesovik, and G. Blatter, Generating spin-entangled electron pairs in normal conductors using voltage pulses, Phys. Rev. B **72**, 245314 (2005).
[67] K. V. Bayandin, G. B. Lesovik, and T. Martin, Energy entanglement in normal metal–superconducting forks, Phys. Rev. B **74**, 085326 (2006).
[68] N. K. Allsopp, V. C. Hui, C. J. Lambert, and S. J. Robinson, Theory of the sign of multi-probe conductances for normal and superconducting materials, J. Phys.: Condens. Matter **6**, 10475 (1994).
[69] J. M. Byers and M. E. Flatté, Probing Spatial Correlations with Nanoscale Two-Contact Tunneling, Phys. Rev. Lett. **74**, 306 (1995).
[70] J. Torrès and T. Martin, Positive and negative Hanbury-Brown and Twiss correlations in normal metal-superconducting devices, Eur. Phys. J. B **12**, 319 (1999).
[71] G. Deutscher and D. Feinberg, Coupling superconducting-ferromagnetic point contacts by Andreev reflections, Appl. Phys. Lett. **76**, 487 (2000).
[72] G. Falci, D. Feinberg, and F. W. J. Hekking, Correlated tunneling into a superconductor in a multiprobe hybrid structure, Europhys. Lett. **54**, 255 (2001).
[73] R. Mélin and D. Feinberg, Transport theory of multiterminal hybrid structures, Eur. Phys. J. B **26**, 101 (2002).
[74] R. Mélin and D. Feinberg, Sign of the crossed conductances at a ferromagnet/superconductor/ferromagnet double interface, Phys. Rev. B **70**, 174509 (2004).
[75] R. Mélin, C. Benjamin, and T. Martin, Positive cross correlations of noise in superconducting hybrid structures: Roles of interfaces and interactions, Phys. Rev. B **77**, 094512 (2008).
[76] A. Freyn, M. Flöser and R. Mélin, Positive current cross-correlations in a highly transparent normal-superconducting beam splitter due to synchronized Andreev and inverse Andreev reflections, Phys. Rev. B **82**, 014510 (2010).
[77] M. Flöser, D. Feinberg, and R. Mélin, Absence of split pairs in cross correlations of a highly transparent normal metal–

superconductor–normal metal electron-beam splitter, Phys. Rev. B **88**, 094517 (2013).

[78] A. F. Andreev, Thermal conductivity of the intermediate state of superconductors, Sov. Phys. JETP **20**, 1490 (1965) [J. Exp. Theor. Phys. **47**, 2222 (1964)].

[79] L. Bretheau, Ç. Ö. Girit, D. Esteve, H. Pothier and C. Urbina, Tunnelling spectroscopy of Andreev states in graphene, Nature (London) **499**, 319 (2013).

[80] L. Bretheau, Ç. Ö. Girit, C. Urbina, D. Esteve, H. Pothier, Supercurrent Spectroscopy of Andreev States, Physical Review X **3**, 041034 (2013).

[81] J. Schindele, A. Baumgartner, R. Maurand, M. Weiss, and C. Schönenberger, Nonlocal spectroscopy of Andreev bound states Phys. Rev. B **89**, 045422 (2014).

[82] D. G. Olivares, A. L. Yeyati, L. Bretheau, Ç. Ö. Girit, H. Pothier, C. Urbina, Dynamics of quasiparticle trapping in Andreev levels, Phys. Rev. B **89**, 104504 (2014).

[83] C. Janvier, L. Tosi, L. Bretheau, Ç. Ö. Girit, M. Stern, P. Bertet, P. Joyez, D. Vion, D. Esteve, M. F. Goffman, H. Pothier, and C. Urbina, Coherent manipulation of Andreev states in superconducting atomic contacts, Science **349**, 1199 (2015).

[84] J. Gramich, A. Baumgartner, and C. Schönenberger, Resonant and Inelastic Andreev Tunneling Observed on a Carbon Nanotube Quantum Dot, Phys. Rev. Lett. **115**, 216801 (2015).

[85] L. Bretheau, J. I.-J. Wang, R. Pisoni, K. Watanabe, T. Taniguchi and P. Jarillo-Herrero, Tunnelling spectroscopy of Andreev states in graphene, Nat. Phys. **13**, 756 (2017).

[86] J. Gramich, A. Baumgartner, and C. Schönenberger, Andreev bound states probed in three-terminal quantum dots, Phys. Rev. B **96**, 195418 (2017).

[87] B. Dassonneville, A. Murani, M. Ferrier, S. Guéron, and H. Bouchiat, Coherence-enhanced phase-dependent dissipation in long SNS Josephson junctions: Revealing Andreev bound state dynamics, Phys. Rev. B **97**, 184505 (2018).

[88] L. Tosi, C. Metzger, M. F. Goffman, C. Urbina, H. Pothier, S. Park, A. L. Levy Yeyati, J. Nygøard, P. Krogstrup, Spin-Orbit Splitting of Andreev States Revealed by Microwave Spectroscopy, Phys. Rev. X **9**, 011010 (2019).

[89] W. J. Tomasch, Geometrical Resonance in the Tunneling Characteristics of Superconducting Pb, Phys. Rev. Lett. **15**, 672 (1965).

[90] W. J. Tomasch, Geometrical Resonance and Boundary Effects in Tunneling from Superconducting In, Phys. Rev. Lett. **16**, 16 (1966).

[91] W. J. Tomasch and T. Wolfram, Energy Spacing of Geometrical Resonance Structure in Very Thick Films of Superconducting In, Phys. Rev. Lett. **16**, 352 (1966).

[92] W. L. McMillan and P. W. Anderson, Theory of Geometrical Resonances in the Tunneling Characteristics of Thick Films of Superconductors, Phys. Rev. Lett. **16**, 85 (1966).

[93] T. Wolfram and G. W. Lehman, Theory of the Tomasch effect, Phys. Lett. A **24**, 101 (1967).

[94] R. Mélin, F. S. Bergeret, and A. Levy Yeyati, Self-consistent microscopic calculations for nonlocal transport through nanoscale superconductors, Phys. Rev. B **79**, 104518 (2009).

[95] J. Gavoret, P. Nozières, B. Roulet, M. Combescot, Optical absorption in degenerate semiconductors, J. Phys. **30**, 987 (1969).

[96] B. J. Van Wees, K.-M. H. Lenssen and C. J. P. M. Harmans, Transmission formalism for supercurrent flow in multiprobe superconductor-semiconductor devices, Phys. Rev. B **44**, 470 (1991).

[97] J. J. A. Baselmans, A. F. Morpurgo, B. J. van Wees and T. M. Klapwijk, Reversing the direction of the supercurrent in a controllable Josephson junction, Nature (London) **397**, 43 (1999).

[98] C. Caroli, R. Combescot, P. Nozières and D. Saint-James, Direct calculation of the tunneling current, J. Phys. C: Solid State Phys. **4**, 916 (1971).

[99] D. Averin and A. Bardas, Ac Josephson Effect in a Single Quantum Channel, Phys. Rev. Lett. **75**, 1831 (1995).

[100] J. C. Cuevas, A. Martín-Rodero, and A. Levy Yeyati, Hamiltonian approach to the transport properties of superconducting quantum point contacts, Phys. Rev. B **54**, 7366 (1996).

[101] J. C. Cuevas, A. Martín-Rodero, and A. Levy Yeyati, Shot Noise and Coherent Multiple Charge Transfer in Superconducting Quantum Point Contacts, Phys. Rev. Lett. **82**, 4086 (1999).

[102] E. N. Bratus', V. S. Shumeiko, E. V. Bezuglyi, and G. Wendin, Dc-current transport and ac Josephson effect in quantum junctions at low voltage, Phys. Rev. B **55**, 12666 (1997).

[103] K. D. Usadel, Generalized Diffusion Equation for Superconducting Alloys, Phys. Rev. Lett. **25**, 507 (1970).

[104] S. B. Kaplan, C. C. Chi, D. N. Langenberg, J. J. Chang, S. Jafarey, and D. J. Scalapino, Quasiparticle and phonon lifetimes in superconductors, Phys. Rev. B **14**, 4854 (1976).

[105] R. C. Dynes, V. Narayanamurti, and J. P. Garno, Direct Measurement of Quasiparticle-Lifetime Broadening in a Strong-Coupled Superconductor, Phys. Rev. Lett. **41**, 1509 (1978).

[106] J. P. Pekola, V. F. Maisi, S. Kafanov, N. Chekurov, A. Kemppinen, Yu. A. Pashkin, O.-P. Saira, M. Möttönen, and J. S. Tsai, Environment-Assisted Tunneling as an Origin of the Dynes Density of States, Phys. Rev. Lett. **105**, 026803 (2010).

[107] O.-P. Saira, A. Kemppinen, V. F. Maisi, and J. P. Pekola, Vanishing quasiparticle density in a hybrid Al/Cu/Al single-electron transistor, Phys. Rev. B **85**, 012504 (2012).

[108] F. W. J. Hekking and Yu. V. Nazarov, Interference of Two Electrons Entering a Superconductor, Phys. Rev. Lett. **71**, 1625 (1993).

[109] F. W. J. Hekking and Yu. V. Nazarov, Subgap conductivity of a superconductor–normal-metal tunnel interface, Phys. Rev. B **49**, 6847 (1994).

[110] G. E. Blonder, M. Tinkham and T. M. Klapwijk, Transition from metallic to tunneling regimes in superconducting microconstrictions: Excess current, charge imbalance, and supercurrent conversion, Phys. Rev. B **25**, 4515 (1982).

[111] D. Gosselin, G. Hornecker, R. Mélin and D. Feinberg, Phase-sensitive transport at a normal metal-superconductor interface close to a Josephson junction, Phys. Rev. B **89**, 075415 (2014).

[112] P. W. Anderson, New method in the theory of superconductivity, Phys. Rev. **110**, 985 (1958).

[113] P. W. Anderson, Random-phase approximation in the theory of superconductivity, Phys. Rev. **112**, 1900 (1958).

[114] I. O. Kulik, O. Entin-Wohlman and R. Orbah, Pair susceptibility and mode propagation in superconductors: A microscopic approach, J. Low Temp. Phys. **43**, 591 (1981).